Master's thesis

NTNU
Norwegian University of Science and Technology
Faculty of Information Technology and Electrical Engineering
Department of Electric Power Engineering

Håvard Dahl Mediaas

Contribution of Energy Storage to Generation Adequacy

Master's thesis in Energy and Environmental Engineering
Supervisor: Vijay Venu Vadlamudi
June 2020

NTNU
Norwegian University of Science and Technology

Håvard Dahl Mediaas

Contribution of Energy Storage to Generation Adequacy

Master's thesis in Energy and Environmental Engineering
Supervisor: Vijay Venu Vadlamudi
June 2020

Norwegian University of Science and Technology
Faculty of Information Technology and Electrical Engineering
Department of Electric Power Engineering

NTNU
Norwegian University of
Science and Technology

Abstract

The objective of this thesis is to evaluate the contribution of battery energy storage systems to generation adequacy by applying Monte Carlo simulation and capacity value quantification. As a response to the increasing global energy demand and environmental problems, the installed wind power capacity has grown rapidly over the last years. The intermittent characteristics of wind challenge the reliability of the power system. With the recent advances in battery technology, battery energy storage systems may be an essential key in exploiting wind energy. Probabilistic power system reliability studies, a highly developed field for evaluating reliability of power systems with uncertain behaviour, are needed for efficient planning of complex power systems, especially the ones with high penetration of renewable energy resources. The introduction of intertemporal characteristics due to the presence of renewable energy resources and battery energy storage will introduce new considerations to the reliability assessment, requiring sequential Monte Carlo simulation techniques. This thesis explores these aspects.

The thesis focuses on incorporating quantification of capacity value in generation adequacy assessment of power systems consisting of traditional and wind power generation with the inclusion of battery energy storage systems. Probabilistic generation adequacy indices (LOLE and EENS)[1] are applied to obtain the capacity value metric ELCC[2]. The algorithmic approaches for calculating ELCC have been implemented in existing indigenous MATLAB scripts for generation adequacy assessment using the Monte Carlo state transition simulation method, while scripts for wind speed sampling, and battery energy storage modelling together with operation strategies have been developed. The scripts are tested on two test systems - the Roy Billinton Test System (RBTS) and the IEEE Reliability Test System (RTS).

[1] Loss of Load Expectation, Expected Energy Not Served
[2] Equivalent Load Carrying Capability

Four different energy storage operation strategies and two methods of calculating the ELCC metric are evaluated. It is clearly observed that strategies aiming to improve the system reliability provide considerably higher capacity value of battery energy storage systems. Due to EENS considering the severity of LOL[3] events rather than the mere occurrence of LOL, it was found that the EENS is the preferred method of obtaining the ELCC.

[3]Loss of Load

Sammendrag

Formålet med denne avhandlingen er å evaluare bidraget fra batterilargringssystemer på leveringspåliteligheten til kraftsystem ved å anvende Monte Carlo-simulering og kvantifisering av kapasitetsverdi. Den installerte vindkraftskapasiteten har på verdensbasis økt kraftig de siste årene som en reaksjon på det økende energibehovet og miljøproblemene globalt. De tilfeldige og periodiske egenskapene til vind skaper utfordringer for påliteligheten til kraftsystemet. Med fremskrittene innen batteriteknologi kan batterilagringssystemer være en essensiell del av løsningen i utnyttelsen av vindkraft. Probabilistiske pålitelighetsstudier for kraftsystemer, et svært etablert fagfelt innen leveringspålitelighetsevalueringer av kraftsystemer med tilfeldig og usikker atferd, er nødvendige for effektiv planlegging av komplekse kraftsystemer, spesielt for kraftsystemer med en stor andel av fornybare energikilder. Innføringen av intertemporale karakteristikker på grunn av tilstedeværelsen av fornybare energiressurser og batterilagringssystemer vil introdusere nye betrakninger til leveringspålitelighetsevalueringen, som krever sekvensielle Monte Carlo-simuleringsteknikker.

Avhandlingen fokuserer på å inkorporere kvantifisering av kapasitetsverdi i evalueringen av leveringspålitelighet for kraftsystem bestående av konvensjonelle generatorer og vindkraftproduksjon med inkludering av batterilagringssystemer. Probabilistiske indekser for leveringspålitelighet (LOLE og EENS)[4] anvendes for å beregne kapasitetsbidraget med indeksen ELCC[5]. Den algoritmiske prosedyren for utregningen av ELCC har blitt implementert i den eksisterende, interne MATLAB-kodene for evaluering av kraftsystemers leveringspålitelighet ved anveding av Monte Carlo-simuleringsmetoden kjent som *state transition*, mens koder for sampling av vinddata og modellering av batterilagringssystemer og driftsstrategier har blitt utviklet. De resulterende kodene er testet på standardtestsystemene for pålitelighetsstudier av kraftsystemer, kjent som *Roy Billinton Test System* og *IEEE Reliability Test System*.

[4] Loss of Load Expectation, Expected Energy Not Served
[5] Equivalent Load Carrying Capability

Fire driftsstrategier for energilagring og to metoder for utregning av ELCC blir evaluert. Det er tydelig observert at driftsstrategiene med mål om å forbedre systemets pålitelighet gir betydelig høyere kapasitetsverdi for batterilagringssystemet. Det ble også oppdaget at EENS-metoden for utregning av ELCC var den foretrukne metoden, ettersom EENS vurderer alvorlighetsgraden ved tap av last snarere enn forekomsten av lasttapssituasjoner.

Acknowledgement

This thesis is the conclusion of my Master of Science (MSc) degree in Energy and Environmental Engineering at the Department of Electric Power Engineering at the Norwegian University of Science and Technology (NTNU). The thesis deals with concepts from the field of Power System Reliability (PSR), and the work was performed under the supervision of Associate Professor Vijay Venu Vadlamudi at the Department of Electric Power Engineering, NTNU. I am very grateful for everything I have learned during my years at NTNU.

I would like to thank my supervisor, Associate Professor Vijay Venu Vadlamudi, with the sincerest of gratitude for great guidance, encouragement and the knowledge I have gained on PSR over the course of the last year. Your availability, input and commitment during these troublesome times have been invaluable and are highly appreciated.

I want to thank Mom and Dad for always supporting me. Thank you, Sindre, for helping with the monumental and tedious work of proofreading, and for always raising the bar and setting an example I can strive for. Last, but not least, I want to thank Elin Overrein for all the support, laughter and happiness you have given me over the last 7 years. I could not have done it without you.

Contents

List of Figures

List of Tables

Abbreviations

ARMA	=	Auto Recursive Moving Average
BESS	=	Battery Energy Storage System
CV	=	Capacity Value
CYPL	=	Constant Yearly Peak Load
DPL	=	Daily Peak Load
ECC	=	Equivalent Conventional Capacity
EFC	=	Equivalent Firm Capacity
EENS	=	Expected Energy Not Served
ELCC	=	Equivalent Load Carrying Capability
FOR	=	Forced Outage Rate
HL	=	Hierarchical Level
HPL	=	Hourly Peak Load
LOL	=	Loss of Load
LOLE	=	Loss of Load Expectation
LOLF	=	Loss of Load Frequency
MCS	=	Monte Carlo Simulation
MTTF	=	Mean Time To Failure
MTTR	=	Mean Time To Repair
PF	=	Power Flow
PV	=	Photovoltaic
PSR	=	Power System Reliability
RBTS	=	Roy Billinton Test System
RE	=	Renewable Energy
RES	=	Renewable Energy Source
RTS	=	Reliability Test System
TTF	=	Time To Failure
TTR	=	Time To Repair
WPL	=	Weekly Peak Load
WTG	=	Wind Turbine Generator

Chapter 1

Introduction

1.1 Background

The global energy demand is ever growing; the global environmental issues has continuously grown over the last decades, due to fossil energy sources traditionally covering the largest part of the consumption. Thus, there is a crucial need of Renewable Energy Sources (RES). In a reaction to the world's vast environmental problems, the installed RES capacity has rapidly increased from year to year, with wind power as the largest growing installed RES over the last decade together with solar PV electricity generation [1, 2]. The security of supply and power system flexibility are challenged by the increased amount of renwables, phaseout of non-renewable resources, and change of energy consumption and demand, as intermittent[1] characteristics are introduced to the power system [4]. With technological advances and falling costs over the last years, Battery Energy Storage Systems (BESS) may be an essential key in controlling the intermittency and exploiting wind power generation [5]. With consumers expecting continuously available energy, there is a balancing act between the reliability and economic aspects. Hence, a tool based on objective criteria is required in order to conduct a comprehensive assessment of the necessary balancing between these aspects.

[1] Not continuous, coming and going in intervals. [3]

The field of Power System Reliability (PSR) assessment is highly developed. Deterministic criteria have historically been used for assessing PSR, but are not able to capture the random nature of a power system [6]. Probabilistic assessment techniques capture the uncertainties, as well as provide more information than deterministic methods [7]. However, the probabilistic reliability indices can be difficult to interpret, as they reflect on the estimated possibility of a system behaviour. Probabilistic methods can be categorised as analytical or simulation based. Analytical PSR methods may require assumptions to simplify complex system effects and processes, while simulation based methods can in theory incorporate the system complexity [8]. Most simulation methods are based on Monte Carlo Simulation (MCS), which provide the opportunity to include vast amount of modelling details in the assessment [9].

Probabilistic PSR indices are used reflect on the reliability level of a power system. The concepts of Capacity Value (CV) are applied to examine the contribution of including an additional generation unit or implementing energy storage to the overall system adequacy. The CV of a energy source depends on type of technology, the availability of the unit, and the overall system characteristics. It is important to note that the calculated CV metric of a generation unit is specific for each different system, hence change if other system component parameters are modified.

1.2 Scope

This thesis is an addition to the computational tools in the ongoing project of building a comprehensive framework for conducting PSR assessment, at the Department of Electric Power Engineering at NTNU. The objective is to evaluate the contribution of BESS to the reliability of generation systems with integrated wind power generation. Traditional reliability metrics such as Loss of Load Expectation (LOLE) and Expected Energy Not Served (EENS) are used to quantify the CV with help of MCS. The thesis is partly an extension of the Master's theses [10, 11] from the Department of Electric Power Engineering at NTNU, as the developed MCS software for generation adequacy studies in [10] is combined and modified with parts of the analytical wind power generation CV evaluation

software of [11].

The main concepts applied are well-established from the field of PSR assessment, such as LOLE, EENS and Effective Load Carrying Capability (ELCC). The studies of this thesis are limited to generation adequacy evaluations, i.e. HL-I (Hierarchical Level I) studies.

A significant part of the project work has been to integrate and modify the MATLAB scripts from [10, 11] to include quantification of CV in the form of the ELCC metric, as well as developing new scripts for the modelling of BESS and sampling of wind speed series to obtain the overall ELCC of a generation system which consists of traditional generators, RES such as wind, and BESS. In addition, some time was spent in gaining insight into the sampling of wind speed with Weibull distribution, and the theoretical and algorithmic aspects of CV and its quantification.

The thesis mainly focuses on building the MATLAB scripts for obtaining the ELCC of systems consisting of traditional and wind generators together with the inclusion of BESS, performing relevant sensitivity analyses, and comparing the results and conclusions with findings from literature. Four BESS operation strategies and two methods of calculating the ELCC are evaluated in the thesis. The standard PSR test systems are applied, hence the Roy Billinton Test System (RBTS) and the IEEE Reliability Test System (RTS). Thus, the thesis does not use real-life case scenarios or data from real-life power systems.

1.3 Thesis Contributions

- The thesis builds on a specialisation project undertaken in Autumn 2019, where the main focus was of achieving a conceptual understanding of the theoretical and algorithmic aspects of PSR assessment and the applications of MCS in power system adequacy assessment. In addition, the significance of battery energy storage modeling was studied and understood.

- The applied methodological CV evaluation approach combines methods and concepts from [10, 11] and relevant literature available on PSR studies, wind modelling and BESS modelling. The conceptual background and applications of the concepts used in the thesis are presented to clarify their features and nuances. Illustrative examples are presented to demonstrate the procedure of applied methods and provide further clarification of the algorithmic aspects.

- The existing in-house MATLAB scripts have been combined and suitably extended to include the algorithmic approaches of calculating the ELCC metrics for the RBTS and the RTS. MATLAB scripts for wind speed sampling utilising the Weibull distribution, BESS modelling, and energy storage operation strategy modelling have been developed. The scripts are released for further internal use and research at the Department of Electric Power Engineering at NTNU.

1.4 Thesis Structure

Chapter 1 - *Introduction*: provides the motivation, background, scope and contributions of the thesis.

Chapter 2 - *Conceptual Background*: presents the essential theory and concepts of generation adequacy assessment, as well as introduces CV quantification with ELCC and the application of MCS. In addition, the modelling concepts of wind power generation and BESS required for generation adequacy studies are presented.

For establishing narrative clarity and with an aim to make this thesis a complete and independent unit in and of itself, much of the content from chapter 2 is a replication of the specialisation project work, with suitable extensions where deemed necessary.

Chapter 3 - *Methodological Approach*: presents the proposed methodology of evaluating the ELCC metric and a simple example to illustrate the approach of the applied method.

Chapter 4 - *Case Study*: presents and discusses the results obtained by applying the proposed methodological approach on the two test systems; several relevant sensitivity analyses are conducted to further investigate applied method.

Chapter 5 - *Conclusion*: summarises the results, provides concluding remarks and suggestions for future work.

Chapter 2

Conceptual Background

This chapter presents the essential concepts of this thesis. The fundamental elements of generation adequacy assessment are considered and the application of Monte Carlo simulation is introduced. In addition, the modelling concepts of wind power generation and battery energy storage systems are presented.

2.1 Power System Reliability

Power system reliability (PSR) is defined as the "*probability that an electric power system can perform a required function under given conditions for a given time interval*" by the International Electrotechnical Commission [12]. Thus, PSR quantifies the system's ability to supply satisfactory electric service for a longer period of time. Measures of disturbance duration, frequency and magnitude within a given time interval indicate how well the system performs its basic function [13].

PSR can be divided in terms of two basic functional aspects; adequacy and security. The two elements can be defined as [14]:

- "*Adequacy*: The ability of the electric system to supply the aggregate electrical demand and energy requirements of customers at all times, taking into account scheduled and reasonably expected unscheduled outages of system elements."
- "*Security*: The ability of the electric system to withstand sudden disturbances such as electric short circuits or unanticipated loss of system elements."

The definitions relate the power system security to the dynamic behaviour of the system, and the power system adequacy to the steady state conditions of the system.

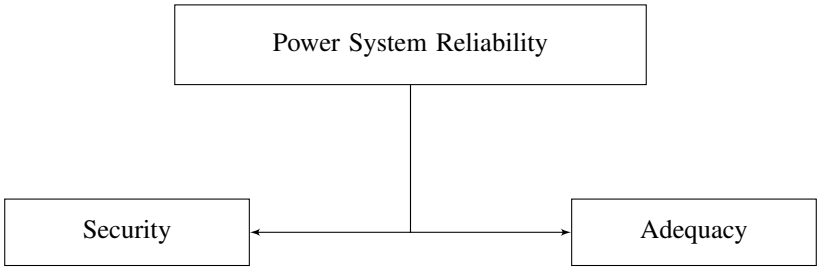

Figure 2.1: The two domains of PSR [6].

Security relates to the transient behaviour of the system. The transient effects are present under different system disturbances, e.g. loss of generation and line faults, as well as when the system state changes [10]. The security assessment evaluates whether the system can remain within the stability limits during the transient phenomena.

A power system adequacy assessment evaluates if there are sufficient electrical facilities to satisfy the load demand under different steady state conditions [15]. The adequacy is typically analysed through Power Flow (PF) simulations, which can vary in complexity based on which electrical facilities are included in the assessment. This thesis only evaluates elementary generation adequacy, hence only includes generation units and load requirements. Transmission and distribution facilities can be included in the assessment for a more complete and throughout system adequacy evaluation.

Through a PSR assessment the system can be classified in a number of different states. The power system can be described as a combination of adequate/inadequate and secure/insec-

ure [16].

- Secure and Adequate: The system is in steady state with the system load requirements satisfied and constraints fulfilled.
- Insecure and Adequate: The system load requirements are satisfied and constraints fulfilled, but the transient stability limits has been exceeded, e.g. due to a contingency. Thus, the system changes to an inadequate state.
- Secure and Inadequate: Violation of system load requirements and/or constraints, yet not in a transient behaviour. In a sense in steady state, however not able to meet the system requirements.
- Insecure and Inadequate: Violation of system load requirements and/or constraints, in addition to exceeding the system's stability limits.

2.1.1 Hierarchical Levels

PSR studies are usually categorised in terms of what functional zone of the power system they are addressing, with associated hierarchical levels (HL) [17]. The functional zones and hierarchical levels are presented in Figure 2.2.

A PSR assessment of HL-I evaluates the generation adequacy and does not include dynamic security. HL-II studies include both generation and transmission facilities, evaluating the ability of the composite system to sufficient supply the system load points [16]. HL-III studies include all three hierarchical segments, assessing the whole system's ability of providing sufficient energy transportation to the end-consumers from the generation facilities. HL-II and HL-III adequacy studies usually ignore the transient effects and only evaluate the steady state requirements of the system [8]. However, even if both the departure and arriving state are adequate, the transient effects may be important in determining whether it is a temporary or static state. Hence, a security evaluation is necessary for a complete PSR study of HL-II and HL-III [16]. This thesis evaluates generation adequacy and only HL-I is relevant, thus the aspects of power system security assessment are not treated further.

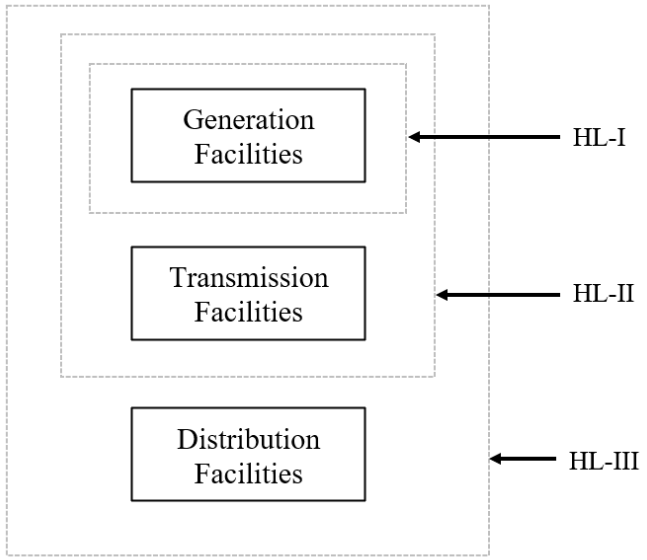

Figure 2.2: Functional zones and hierarchical levels of a power system [18].

HL-I study

HL-I studies only consider the generation facilities and evaluate their ability to produce energy and meet the system load requirement. The energy transportation units, i.e. the transmission and distribution facilities, are not considered and assumed to have perfect reliability. Thus, there are no constraints related to the transferring and transportation of power, meaning eventual power supply interruptions are due to the generation units [19]. A simple representation of a HL-I model is shown in Figure 2.3.

Figure 2.3: Simple HL-I model [18].

2.1.2 Generation Adequacy

Methodologies in PSR studies distinguish between deterministic and probabilistic techniques. The techniques use different mathematical procedures and risk indices to measure the reliability of the system [6]. There are also existing hybrid methods, which are not discussed in this thesis.

Deterministic approaches aim to estimate the available generation and network capacity at some time in the future based on deterministic criteria. The deterministic methods are widely utilised in power system planning, as PSR is an important aspect in the design of the system [7]. The most used deterministic reliability method for PSR is the N-1 criterion, which consider the system as reliable if it can withstand any fixed outage or contingency situation. However, a multiple challenges appear in the deterministic power system studies. The deterministic method does not consider type of generation technology, meaning the unequal probabilities of generation which are present with various sources, e.g. hydro and wind power, are not taken into account. In addition, the uncertainties regarding future power demand are a challenge for deterministic approaches. Thus, there is a need for probabilistic methods, which offers much more information and can handle large sets of possibilities efficiently [7].

Probabilistic approaches aim to estimate the probability that the system are unable to supply demand, considering the stochastic nature of the generation, transmission and distribution resources, as well as the uncertainty associated with the load demand. The probabilistic methods can be classified in two main categories, analytic and simulation based methods [6]. Both methods are based on system states, which are decided based on the availability of the system components.

Analytical Methods

The system is represented by mathematical models in analytical based PSR assessment. The models are typically based on Markov models.

The probabilistic indices are calculated by solving equation sets with the probability and frequency of the system states as variables [9]. The models assume a fitting probability distribution function for the different system components to obtain the random variables of interest [6]. The most common analytical methods are the *state space method*, the *contingency enumeration method* and the *minimal cut set method* [15]. The analytical methods rely on mathematical assumptions to represent the system in a model. Hence, larger and more complex systems require an increase number of assumptions, decreasing the accuracy and realism of the study. In addition, correlation between load and generation can not be implemented in analytical models [11].

Simulation Methods

Simulation techniques consider the mathematical problems from the system representation model as real experiments, capturing the random behaviour in the system. Since the simulations involve random numbers, most methods are based on the Monte Carlo Simulation methodology [9]. MCS provides the opportunity to include a vast amount of details in the assessment. The basics of MCS theory is presented in Section 2.2.

The simulation methods can be classified as either sequential or non-sequential procedures [6]. Non-sequential methods evaluate multiple random time intervals with different system states independently, neglecting the transition between the states. Sequential methods, however, recognise the operating cycle of the system components and the actual transition of system states, providing additional time-dependent PSR indices such as duration and frequency of load loss. The sequential techniques are the only techniques that have the ability to consider models with intertemporal[1] characteristics [6], and should be utilised whenever the system operation depends on history, such as systems with energy storage systems. Hence, this thesis applies sequential simulation techniques for PSR assessment. The main drawbacks with the sequential procedures are the required computational power and time to complete these kinds of simulations [9].

[1] The relationship between past, present and future events or conditions. [20]

Component Unavailability

The system state during a certain time interval is dependent on the availability of the components in the system during the time period. The availability of a unit can be defined as the unit's ability to perform its required function at a given time period [14]. A PSR assessment usually apply the complement of availability, the unavailability, often referred to as the forced outage rate (FOR) of a unit in power system applications. The FOR is mathematically expressed in (2.1), where a component is either classified as working (up) or not working (down) [18]. Note that FOR is the ratio of two time values and not a rate in modern reliability term.

$$FOR = \frac{\lambda}{\lambda + \mu} = \frac{MTTR}{MTTR + MTTF} = \frac{\sum[downtime]}{\sum[downtime] + \sum[uptime]} \tag{2.1}$$

where λ = expected component failure rate
μ = expected component repair rate
$MTTF$ = mean time to failure
$MTTR$ = mean time to repair

Elements in a MCS Generation Adequacy Assessment

The fundamental elements in a generation adequacy assessment are presented in Figure 2.4. For each time increment over a simulation year, the simulation creates a generation model by determining the state of each generation unit. The generation model is convolved with a load model to form a risk model. The risk model investigates if the available capacity of power supply is sufficient to meet the load requirements according to (2.2). If the load demand is not satisfactory supplied, the system state is recorded as a failure and the severity is calculated with (2.3) [10]. Adequacy indices are calculated for each simulation year.

$$\sum_{i=1}^{n} P_{g,i} \geq \sum_{j}^{k} P_{load,j} \tag{2.2}$$

$$\text{Energy not served} = \left(\sum_{j}^{k} P_{load,j} - \sum_{i=1}^{n} P_{g,i} \right) \Delta t \tag{2.3}$$

By conducting simulation over the same simulation time period N number of times, estimates of the system indices can be calculated as the mean of computed indices from all N simulation years. By increasing the sample size N, the variance of the indices' estimated mean decrease, meaning the precision of the MCS indices of increase. Thus, it can be assumed that if N is sufficiently large, the estimated mean value of system indices is approximately equal to the true mean of the indices' distribution [10].

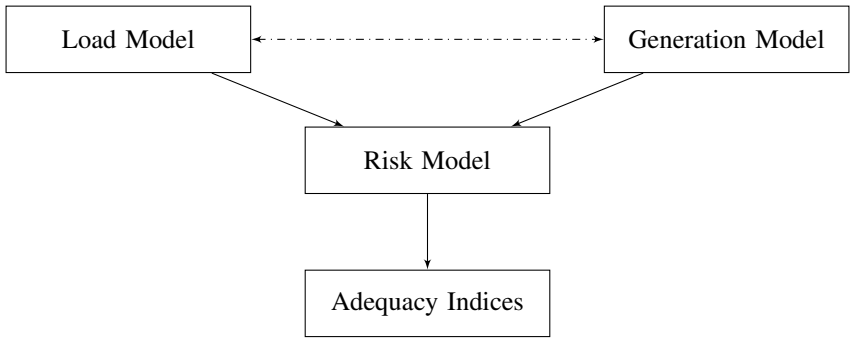

Figure 2.4: Elements in a generation adequacy assessment, based on [18].

2.1.3 Indices

The most common PSR indices are based on Loss of Load (LOL) events in the system. These events are associated with insufficient generation in HL-I studies. The basic adequacy indices are Loss of Load Expectation (LOLE), Loss of Load Probability (LOLP) and Loss of Load Frequency (LOLF) [21]. These indices reflect on the frequency and probability of loss of load events. However, they do not reflect on the severity of the LOL events [18]. Severity based indices, e.g. Expected Energy Not Served (EENS), quantify the LOL severity. The following presented formulations and mathematical expressions of indices are based on formulations presented in [10] and [18].

The LOLE gives the expected number of time units in which the system experiences LOL. The LOLE index is commonly specified in hours/year or days/year. In (2.6), S is the set of system states in which the system has LOL. p_i is the probability of the occurrence of the failure state. The probabilities of the system states of S are summarised and multiplied with the evaluation time period T. T should be a specified number of time increments per period depending on time period, where days/year is obtained by using a DPL model and hours/year for use of the HPL model.

$$LOLE = \sum_{i \in S} p_i \cdot T \tag{2.4}$$

The mathematical expression for LOLE when MCS is applied has a different format. The system states are sampled in the simulation, with a state obtained for each time increment of a simulation year. Usually, multiple years are simulated in one simulation. The reliability indices are found as averages of the yearly indices, meaning the sum of yearly indices are divided by the number of simulation years. The LOLE for MCS is given in (2.5).

$$LOLE_{MCS} = \frac{\sum_{i=1}^{N} (\sum_{j=1}^{M} x_j \cdot \Delta t)}{N} \tag{2.5}$$

One simulation year consists of M time increments, each increment with duration of Δt. The outcome, x_j, of each time increment is given by either a one or a zero. An outcome of one represents a LOL event for the associated system state, while a zero represents an adequate state. Each outcome multiplied with the time increment is summed up, before summing all the number simulation years, N. The final indices are obtained by dividing the sum by N.

LOLP gives the probability that an LOL event will occur during the time of period studied. It is calculated as the sum of probabilities of system states with LOL, mathematically expressed in (2.6).

$$LOLP = \sum_{i \in S} p_i \tag{2.6}$$

The LOLP index for MCS is a "re-engineered" version, with the $LOLP_{MCS}$ found simply

by dividing the $LOLE_{MCS}$ with M, the number of time increments over a year [16].

$$LOLP_{MCS} = \frac{\sum_{i=1}^{N}(\sum_{j=1}^{M} x_j \cdot \Delta t)}{N \cdot M} \tag{2.7}$$

In addition to the "re-engineered" LOLP in (2.7), there is a general way to consider LOLP in MCS. Each generated state from the simulation has a probability of occurrence. As in (2.6), the probability of the generated failure states can be summed up to the LOLP.

LOLF gives the frequency of system failures. A new system state with LOL is counted whenever there is a transition to a state in the set of failure states, S, from a adequate state, i.e. a state outside of S. In (2.8), F_i is the frequency of departure from any failure state $i \in S$, while f_i denotes the frequency of transitions between two system states with LOL, i.e. two states in the set of failure states S.

$$LOLF = \sum_{i \in S}(F_i - f_i) \tag{2.8}$$

LOLF in the MCS framework is defined in (2.9). The variable z_i is set to one if the LOL state of x_i was preceded by an adequate state x_{i-1}. If not, z_i is set to zero. The variable is summed up through all N simulation years. Thus, $LOLF_{MCS}$ is the average z_i of all the number of simulation years.

$$LOLF_{MCS} = \frac{\sum_{i=1}^{N} z_i(x_{i-1}, x_i)}{N}, \text{ with } z = \begin{cases} 1 & \text{if}(x_{i-1} = 0) \cap (x_i = 1) \\ 0 & \text{if}(x_{i-1} = 1) \cap (x_i = 1) \\ 0 & \text{if}(x_{i-1} = 1) \cap (x_i = 0) \\ 0 & \text{if}(x_{i-1} = 0) \cap (x_i = 0) \end{cases} \tag{2.9}$$

The severity index EENS is commonly used, and is equal to the loss of energy expectation index from studies of HLI. The mathematical expression foe EENS, presented below in (2.10), is similar to the LOLE expression, except the inclusion of C_i. C_i gives the severity of the energy lost. Note that T has to be given in hours/year in order to obtain normal

energy quantity.

$$EENS = \sum_{i \in S} p_i \cdot C_i \cdot T \tag{2.10}$$

The weighting factor is included in equation (2.5) to make the expression for EENS in MCS studies, presented in (2.11).

$$EENS_{MCS} = \frac{\sum_{i=1}^{N} (\sum_{j=1}^{M} x_j \cdot C_j \cdot \Delta t)}{N} \tag{2.11}$$

2.1.4 Capacity Value

Capacity Value (CV), also often referred to as capacity credits, represents the contribution of a given generation unit to the overall system adequacy [22]. In generation expansion planning, LOLE and EENS can be used to examine the effect of new generation units on the system reliability. It can be useful to quantify the contribution from the added generation units in meeting increasing load in the future. CV metrics are often estimated by using methods based on the traditional reliability indices LOLE, LOLP and EENS [23, 24, 25]. The concept of of CV was developed by Garver in 1966 [26] through Effective Load Carrying Capability (ELCC), and is arguably the most recognised CV metric [22, 23, 24, 27]. Other commonly used metrics such as Equivalent Firm Capacity (EFC) and Equivalent Conventional Capacity (ECC) are not investigated further in this thesis.

Effective Load Carrying Capability

ELCC reflects on the possible increase in load demand a power system can handle if an additional generation unit is implemented. It was initially used in generation expansion for capacity contribution assessment of added conventional generation units, and is of late being adopted for renewable energy contribution assessment, e.g. wind power [22, 28, 29] and energy storage systems [23, 25, 30]. ELCC is suitable tool for assessing the PSR contribution of conventional generation versus RES, as the ELCC values, i.e. possible increase in system load demand, can be compared against each other.

The ELCC calculation approach is presented in (2.12) and (2.13) using LOLE as the benchmark, based on [11] and [31]. This thesis applies ELCC calculation with both LOLE and EENS. The EENS based approach uses the same notation as the LOLE based approach, meaning the LOLE metric can be swapped with the EENS metric in the equations and explanation below. The equations evaluates the LOLE of the old existing system, $LOLE_E$, versus the LOLE of the potential system, $LOLE_P$, which includes the generation capacity of the additional generation unit, i.e. the generation unit that is being assessed.

$$LOLE_E = LOLE_P \tag{2.12}$$

$$\sum_{i=1}^{n} P_i \left(X_E > C_E - L_i\right) = \sum_{i=1}^{n} P_i \left(X_P > (C_E + C_A) - (L_i + \Delta L)\right) \tag{2.13}$$

where:

$LOLE_E$	=	LOLE of the existing system
$LOLE_P$	=	LOLE of the potential system
L_i	=	Load condition during time increment i [MW]
ΔL	=	Extra load that can be served by the potential system
n	=	Total number of time increments in the evaluation period
C_E	=	Total possible generation capacity of the existing system
C_A	=	Maximum possible capacity of the added generation unit

At each time increment i, $P_i \left(X_E > C_E - L_i\right)$ and $P_i \left(X_P > (C_E + C_A) - (L_i + \Delta L)\right)$ denote the LOL probability of the existing and potential systems, respectively.

The calculation of $LOLE_P$ is executed by iteratively increasing the extra load ΔL until the two LOLE values are equal. When they are equal, the corresponding ΔL represents the additional load the system can handle when the extra generation unit with maximum capacity C_A is added. Thus, ΔL is the quantification of ELCC for that specific generation unit in that specific system. Note that a specific generator can have different ELCC values for different systems, as both pre-existing reliability level and the relative size of the added generation unit to the existing generation system influence the ELCC [25]. The ELCC value can also be presented relative to the capacity of the added generation unit, shown in

Equation (2.14) [31].

$$ELCC = \frac{\Delta L}{C_A} \times 100\% \tag{2.14}$$

There are also non-iterative methods of calculating the ELCC, e.g. the curve-fitting method described by Garver [26]. This method is not applied in this thesis and will not be discussed further. The algorithmic approach utilised in this thesis for calculating the ELCC based on LOLE is presented in Figure 2.5.

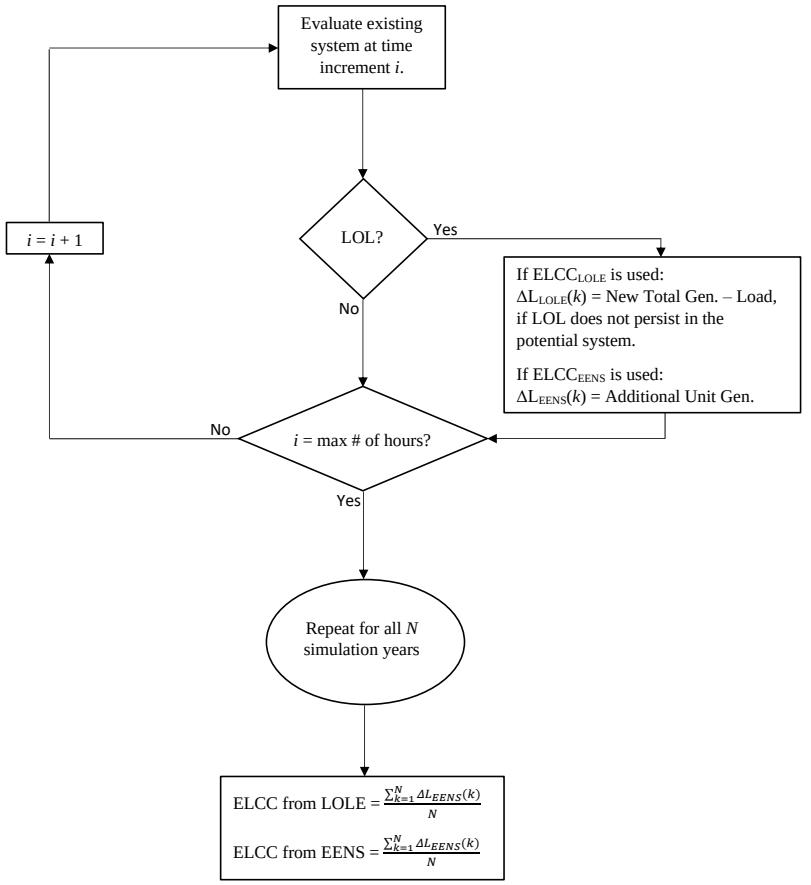

Figure 2.5: The flowchart of the ELCC calculation algorithm.

In Figure 2.5, intended to be self-explanatory, the evaluation of whether the existing system at time increment i encounters a LOL condition is made on the basis of MCS. The generation profile at time increment i is obtained by drawing suitable random numbers for each generator; the generation system state for this time increment is then the summation of capacities of all the generators that are known be in an available state from the drawing of random numbers. The generation system state is evaluated as belonging to a LOL state or not by comparing the cumulative generation capacity of this state against the load demand in the specified time increment i.

- If there is no LOL in this system state, then the time increment is updated to $i + 1$.
- If there is LOL in this system state and $ELCC_{LOLE}$ is used, then a check is performed to see if LOL persists in spite of adding the new generation unit, for which the ELCC is to be determined, in this time increment; If LOL does not persist, then ΔL_{LOLE} is calculated as the difference between the new total generation and the load demand of this increment. If LOL persists, then ΔL_{LOLE} is left uncalculated. Finally, the time increment is updated to $i + 1$.
- If there is LOL in this system state and $ELCC_{EENS}$ is used, ΔL_{EENS} of this time increment is set as the generation of the added unit. This applies for both when the LOL persists and does not persist. Then, the time increment is updated to $i + 1$.

If all the time increments in a simulation year are covered in the above way, a new simulation year is begun until the total number of simulation years is reached. ELCC is then calculated as the average mean of all the accumulated ΔL values. An example is shown next to illustrate the steps of the algorithm.

Illustrative Example

A simple example of two-state model generation system with three conventional generators, G_1 and G_2 with 2 MW capacity each, and G_3 of 1 MW, is considered. An additional generation unit with generation capacity of 1.5 MW is assessed. The system is evaluated over three simulation years consisting of five time increments each, with the aim of calculating ELCC of the additional unit based on the system LOLE and the EENS. The same load profile for each simulation year consisting of five time increments is considered. First time increment has 4.2 MW load demand, second time increment has 4.1 MW load demand, third time increment has 4.5 MW load demand, fourth time increment has 4.4 MW load demand, and fifth time increment has 4.3 MW load demand. Table 2.1 below shows the availability of the generation units, the generation profile of the existing and the potential systems, the system load, whether or not a LOL event occurs at a specific time in the existing system, and the required additional load for LOL to occur in the potential system. The columns in Table 2.1 provide the following information:

- Column 1 with heading time increment.
- Column 2 is a result of identifying generator states of the system by drawing random numbers.
- Column 3 is the total available generation capacity based on the identified system state.
- Column 4 is the load demand of the corresponding time increment for the simulation year.
- Column 5 is the result of the check if LOL occurs, i.e., LOL occurs if the value of column 4 is greater than that of column 3.
- Column 6 is the result of drawing a new random number to assign a status to the new generator for which ELCC is to be determined.
- Column 7 is the total available generation capacity based on the new identified system state (by including the status of the new generator).

- Column 8 is the difference between the value of column 7 and that of column 4. If there is a negative value, then 0 is used instead of the negative value.
- Column 9 is the difference between the new total power generation and the old total power generation based on the identified generator state in column 6. It is the difference between the value of column 7 and that of column 3.

The additional load required is summed up after each simulation year.

The ELCC values of this example system are calculated as the averages over the simulation years, thus:

$$ELCC_{LOLE} = \frac{\sum \Delta L}{\text{\# simulation years}} = \frac{1.5\,\text{MW} + 1.0\,\text{MW} + 1.6\,\text{MW}}{3} = 1.37\,\text{MW}$$
$$ELCC_{EENS} = \frac{\sum \Delta L}{\text{\# simulation years}} = \frac{4.5\,\text{MW} + 3.0\,\text{MW} + 4.5\,\text{MW}}{3} = 4.00\,\text{MW}$$

Note that a large number of samples, i.e. large number of simulation years consisting of a large number of time increments, are needed in order for the simulations to converge and calculate a reasonable realistic value.

Table 2.1: Illustrative example of ELCC calculation with simulation method.

Time i	Generator Availability {G1, G2, G3}	Total Generation [MW]	Load [MW]	LOL [Y/N]	New Unit Availability	New Total Generation [MW]	ΔL_{LOLE} [MW]	ΔL_{EENS} [MW]
			Year 1					
1	1,1,1	3	4.2	Y	1	4.5	0.3	1.5
2	1,1,1	5	4.1	N	1	6.5	0	0
3	1,1,0	4	4.5	Y	1	5.5	1.0	1.5
4	1,1,1	5	4.4	N	0	5	0	0
5	0,1,1	3	4.3	Y	1	4.5	0.2	1.5
			Sum of Additional Load, Year 1				1.5	4.5
			Year 2					
1	1,1,1	5	4.2	N	0	5	0	0
2	0,1,1	3	4.1	Y	0	3	0	0
3	1,1,0	4	4.5	Y	1	5.5	1.0	1.5
4	1,0,1	3	4.4	Y	0	3	0	0
5	1,0,0	2	4.3	Y	1	3.5	0	1.5
			Sum of Additional Load, Year 2				1.0	3.0
			Year 3					
1	1,0,1	3	4.2	Y	1	4.5	0.3	1.5
2	1,1,1	5	4.1	N	1	6.5	0	0
3	1,0,1	3	4.5	Y	0	3	0	0
4	0,1,1	3	4.4	N	1	4.5	0.1	1.5
5	1,1,0	4	4.3	Y	1	5.5	1.2	1.5
			Sum of Additional Load, Year 3				1.6	4.5

2.2 Monte Carlo Simulation Basics

MCS is a tool used for sampling system states to develop operation scenarios that reflect on the behaviour of the system evaluated. The random numbers are sampled from probability distributions and used to classify the transition and state of each considered system component, thus creating different system states for the evaluated time increments over the period of time studied. As mentioned in earlier, the MCS methods can be classified as non-sequential or sequential methods. The non-sequential methods samples the system state of each time increment randomly, while the system states obtained with the sequential methods depends on the previous system states. The system state is given by the combination of the individual components' states. The system states can be expressed by a state vector, $\mathbf{S} = \{S_1,\ S_2,\ \ldots\ S_n\}$, where the n state variables represent the state of the n individual components in the system. The components' states can either be represented binary to represent a two-state model, or in the range of $[0, 1]$ if derated states are included in the assessment.

The three most common MCS methods are briefly introduced in the following, based on [10] and [21]. This thesis only applies the state transition method, as the state sampling method is non-sequential and [10, p. 121] "unable to provide the true distributions of the indices", and because the state duration method requires longer computational time than the state transition method. Thus, the state sampling method and state duration method will not be discussed any further after section 2.2.1 and 2.2.2.

2.2.1 State Sampling

The state sampling technique is a non-sequential method that generates a random number for each component in the system independently from the preceding states. The random number has a value between 0 and 1. The probability of unit unavailability, FOR, is considered for each component. The random number generated for the component is compared to the FOR. If the random number is larger than the FOR value, the component is available. Otherwise, the component is unavailable. Derated states can also be incorporated in the evaluation by including derated state probabilities. Table 2.2 illustrates how the

random number U is compared to the probabilities of the n different possible states of a component.

Table 2.2: Component state probability with derated states.

Component State	Probability Table
Up	$U \geq FOR_n$
⋮	⋮
Derated State i	$FOR_i \leq U \leq FOR_{i+1}$
⋮	⋮
Down	$U \leq FOR_1$

Illustrative Example

As an example for state sampling, a two-state model with four generators of 10 MW and FOR values of 0.3 is considered. A random number is generated each hour for each generator over a sampling time of 10 hours, giving the system states and generating capacities presented in Table 2.3.

Table 2.3: System states with state sampling example

Time	**Random Number** U_1, U_2, U_3, U_4	**System State** S_1, S_2, S_3, S_4	**Generating Capacity [MW]**
0	{0.71, 0.06, 0.13, 0.97}	{1, 0, 0, 1}	20
1	{0.91, 0.37, 0.34, 0.85}	{1, 1, 1, 1}	40
2	{0.11, 0.28, 0.84, 0.95}	{0, 0, 1, 1}	20
3	{0.34, 0.66, 0.00, 0.95}	{1, 1, 0, 1}	30
4	{0.41, 0.57, 0.21, 0.14}	{1, 1, 0, 0}	20
5	{0.33, 0.02, 0.52, 0.43}	{1, 0, 1, 1}	30
6	{0.64, 0.71, 0.55, 0.49}	{1, 1, 1, 1}	40
7	{0.92, 0.04, 0.42, 0.28}	{1, 0, 1, 0}	20
8	{0.12, 0.85, 0.21, 0.34}	{0, 1, 0, 1}	20
9	{0.37, 0.98, 0.07, 0.52}	{1, 1, 0, 1}	30

2.2.2 State Duration

The state duration method is a sequential method, creating a chronological operation cycle of the individual components in the system. The method considers the time to failure (TTF) and time to repair (TTR) distributions of the components, usually assumed to be exponentially distributed. In some cases other distributions are equally applicable [21], this is however not studied in depth in this project since exponentially distribution of TTF and TTR is most commonly used. Random varieties from the distributions are drawn out, creating a state history based on when a failure or a repair occur. The complete state history of the entire system is obtained by combining the individual state history of each component in the system. Initially, all system components are assumed available. If the simulation time period is too short, the starting point may cause overestimation of the reliability. Thus, the state duration method requires simulations over a longer time span. As the reliability indices often require a large quantity of samples to converge, the effect of the initial starting point with available component states often is negligible.

Illustrative Example

A two-state model with two generation units of 10 MW can be considered to illustrate the state duration method. Table 2.4 and 2.5 presents the states of the two units, where '1' indicates that the unit is available and '0' unavailable unit.

Table 2.4: State history of unit 1.

Time	State	TTF	TTR
0	1	4	-
4	0	-	1
5	1	3	-
8	0	-	1
9	1	4	-

Table 2.5: State history of unit 2.

Time	State	TTF	TTR
0	1	2	-
2	0	-	1
3	1	5	-
8	0	-	1
9	1	3	-

This creates the complete system state history with associated generating capacity presented in Table 2.6, with the generating capacity of the system with the associated system state history illustrated in Figure 2.6.

Table 2.6: System states with state duration example

Time [hours]	**System State $\{S_1, S_2\}$**	**Generating Capacity [MW]**
0	{1,1}	20
1	{1,1}	20
2	{1,0}	10
3	{1,1}	20
4	{0,1}	10
5	{1,1}	20
6	{1,1}	20
7	{1,1}	20
8	{0,0}	0
9	{1,1}	20

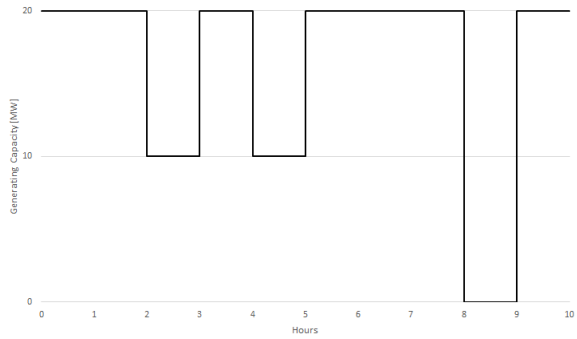

Figure 2.6: System generating capacity with system states from Table 2.6.

2.2.3 State Transition

The state transition method is a sequential method that considers the state transitions of the whole system instead of at component level. The method is valid if all the probability distribution are exponential. It can be proven that the system transition time follow exponential distribution if the components' time to transition are exponential distributed [32], as the total system transition rate is given as the sum of all the transition rates out of the system. Thus, the state transition method is applicable if the times to transition of all the components are exponential distributed.

$$\lambda = \sum_{i=1}^{n} \lambda_i \tag{2.15}$$

The output λ from (2.15) is known as the shape parameter of the system transition time T. T follows an exponential distribution, and expresses the duration of the current system state. It also expresses the minimum of all the components' times to transition, as in (2.16).

$$\mathbf{T} = min\{T_1,\ T_2,\ ...\ T_n\} \tag{2.16}$$

The time of the next system transition can be denoted as t_0. The probability that the transition at t_0 from the current state is to a specific system state j, is given by the conditional probability in (2.17).

$$P_j = P(T_j = t_0 | T = t_0) = \frac{P(T_j = t_0 \cap T = t_0)}{P(T = t_0)} \tag{2.17}$$

Because both T and T_j are assumed exponentially distributed, as required in the state transition method, (2.17) can be rewritten as the transition rate of state j divided by the total sum of transition rates in the system, expressed in (2.18).

$$P_j = \frac{\lambda_j}{\sum_{i=1}^{n} \lambda_i} \tag{2.18}$$

A system state transition can be caused by a state transition of any component. If the system have n different components, it has n possible states [32]. The system must eventually reach one of these states, hence making the sum of system state probabilities equal to one, as shown in (2.19).

$$\sum_{i=1}^{n} P_i = 1 \tag{2.19}$$

In a simulation process, a uniform random number U_1 in the range [0,1] is generated. This number decides the next system state. An additional uniform random number U_2 is generated to calculated the time until the next transition with (2.20).

$$T_{next} = \frac{-ln(U_2)}{\lambda} \tag{2.20}$$

The system state probabilities are calculated by (2.18), in which the total transition rate from (2.15) have to be used. The probability segment which the random number U_1 is within decides the next system state. E.g. if U_1 falls in the segment of P_j, the result of

state j determining the transition from the current system is the next system state. This is graphically illustrated in Figure 2.7.

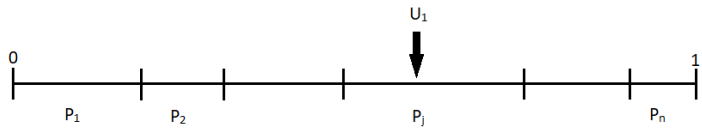

Figure 2.7: Decision of the next system state using the state transition method [16].

Illustrative Example

To illustrate the state transition method, a system consisting of three generators is considered. The state probabilities of the example system are presented in Table 2.7, with all units assumed available at the initial state, meaning the given transition rate in the table is the failure rate for each generator.

Table 2.7: Initial system state probabilities

Generator Number	Transition rate [#/year]	State Probability	Cumulative Probability
#1	3.0	0.30	0.30
#2	2.0	0.20	0.50
#3	5.0	0.50	1.00
Total	10.0	1.00	1.00

After a uniform random number $U_1 = 0.42$ is generated, it is compared with upper limits of the the cumulative probabilities in the above table, meaning the next system state will have generator 2 unavailable. A second uniform random number is generated and equation (2.20) is used to set the time until the next transition. The next system state probabilities are presented in Table 2.8, where the transition rate of generator 2 now is the repair rate of the unit.

Table 2.8: Second system state probabilities

Generator Number	Transition rate [#/year]	State Probability	Cumulative Probability
#1	3.0	0.075	0.075
#2	32.0	0.800	0.875
#3	5.0	0.125	1.000
Total	10.0	1.000	1.000

2.3 Wind Generation Modelling

The overall approaches for evaluating generation adequacy of power systems with presence of wind power are similar for most studies and follow the same steps. However, there are different mathematical models and methods for wind generation modelling in PSR assessment [28, 33, 34]. Several different methods and considerations can be applied in each step, affecting the results from of these steps [11]. Thus, the specific wind model used in a PSR assessment has great affect on the end results. The main steps are:

1. Wind speed modelling.
2. Wind turbine generator modelling.
3. Wind farm modelling.

2.3.1 Wind Speed Modelling

The output power from a Wind Turbine Generator (WTG) depends on the wind speed, which fluctuates randomly with time [35]. Wind power studies therefore require accurate models to predict the varying wind speed. Wind speed is most commonly modeled in hourly wind speed series [36]. The wind speed data can be obtained from historical data or from statistical models and simulation techniques. When using historical data, several years of data from the same location is often utilised to give better predictive accuracy [11]. The Auto Recursive Moving Average (ARMA) time-series model can be used to forecast accurate wind speed data at any particular location [35, 37]. The results in this thesis are obtained with sampled wind speed utilising Weibull distribution based on historical wind

speed data.

Weibull distributions are often used to characterise wind speed distribution and have previously been used in wind power studies [33, 38, 39]. The scale parameter α and shape parameter β can modify the Weibull distribution to represent different distribution characteristics, and can be obtained from collecting historical hourly wind speed data over a significant period of time [35]. The scale parameter α is the mean wind speed, while the shape parameter β relates to the standard deviation of the distribution [40]. The calculation of β can be quite complex and comprehensive. This thesis applies the built-in MATLAB function *wblfit*, which [41] "*... returns the estimates of Weibull distribution parameters (shape and scale), given the sample data ...*" and can also return the 95% confidence interval for the parameter estimates. Another approach of obtaining the shape values is in an iterative manner with the Newton-Raphson method as in [42]. A good initial guess for the shape parameter is 2 [43].

Weibull probability distribution used for wind speed studies is presented in (2.21), where W_s is the wind speed.

$$f\left(W_s\right) = \frac{\beta}{\alpha}\left(\frac{W_s}{\alpha}\right)^{\beta-1} e^{-\left(\frac{W_s}{\alpha}\right)^{\beta}} \quad \text{for} \quad \alpha, \beta, W_s \geq 0 \tag{2.21}$$

This gives the Weibull cumulative probability function in (2.22).

$$F\left(W_s\right) = 1 - e^{-\left(\frac{W_s}{\alpha}\right)^{\beta}} \quad \text{for} \quad \alpha, \beta, W_s \geq 0 \tag{2.22}$$

After determining the values of α and β, the cumulative probability function can be used to determine the wind speed by using the inverse transform method. First, a uniform random number $U \in [0, 1]$ is generated. Then, the cumulative probability function F_{W_s} is set equal to U and the wind speed equation (2.23) is computed [33].

$$W_s = \alpha\left(-ln\left(U\right)^{\frac{1}{\beta}}\right) \tag{2.23}$$

Figure 2.8 presents the Weibull probability distribution with the scale parameter set to 7 m/s and the shape parameter to 2.

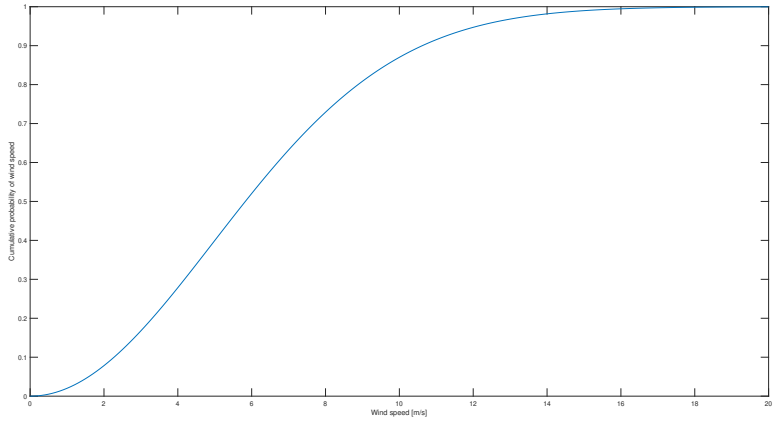

Figure 2.8: Weibull cumulative distribution with $\alpha = 7$ and $\beta = 2$.

2.3.2 Wind Turbine Generator Modelling

A WTG differs from conventional energy sources in that there is a non-linear relation between the WTG output power and the wind speed [33]. The power curve of a WTG can be applied to determine the power output at different wind speeds. Figure 2.9 shows the power curve of a Vestas V90-2MW turbine, which is used for the calculations in this thesis, as it is one of the most installed wind turbines worldwide with over 20,000 installed units [44]. The curve shows that the WTG does not produce power under 4 m/s or over 25 m/s, known as the cut-in and cut-out speed. From the rated wind speed of 15 m/s up to the cut-out wind speed, the turbine produces its rated output power.

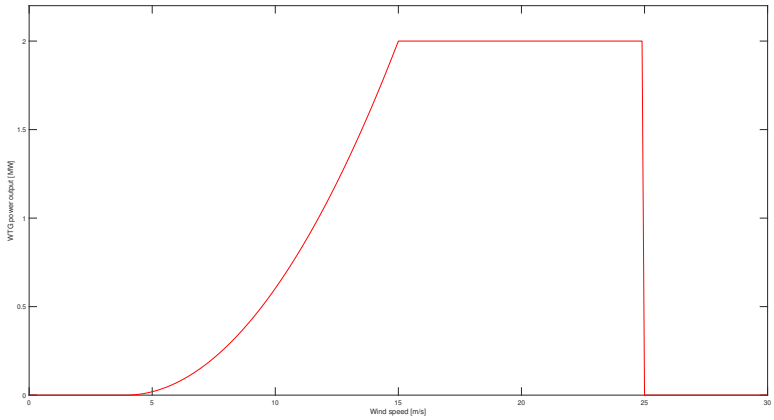

Figure 2.9: Vestas V90-2MW power curve.

The output of a WTG is calculated with (2.24) from [45].

$$P\left(W_s\right) = \begin{cases} 0 & \text{if} \quad 0 \leq W_s < V_{ci} \\ \left(A + B \cdot W_s + C \cdot W_s^2\right) \cdot P_r & \text{if} \quad V_{ci} \leq W_s < V_r \\ P_r & \text{if} \quad V_r \leq W_s < V_{co} \\ 0 & \text{if} \quad W_s \geq V_{co} \end{cases} \tag{2.24}$$

where:

	W_s	=	Wind speed [m/s]
	$P\left(W_s\right)$	=	WTG output power at given wind speed [MW]
	P_r	=	Rated WTG output [MW]
	V_{ci}	=	Cut-in wind speed [m/s]
	V_r	=	Rated wind speed [m/s]
	V_{co}	=	Cut-out wind speed [m/s]

and:

$$A = \frac{1}{(V_{ci} - V_r)^2} \left[V_{ci} (V_{ci} + V_r) - 4 V_{ci} V_r \left(\frac{V_{ci} + V_r}{2 V_r} \right)^3 \right]$$
$$B = \frac{1}{(V_{ci} - V_r)^2} \left[4 (V_{ci} + V_r) \left(\frac{V_{ci} + V_r}{2 V_r} \right)^3 - (3 V_{ci} + V_r) \right]$$
$$C = \frac{1}{(V_{ci} - V_r)^2} \left[2 - 4 \left(\frac{V_{ci} + V_r}{2 V_r} \right)^3 \right]$$

2.3.3 Wind Farm Modelling

After the wind speed modelling and the corresponding WTG output are calculated, the individual turbines are combined for a wind farm model. The wind farm model provides the total produced wind power for each simulated time increment. This thesis uses a simplified wind farm model, and hence does not consider the wake effect or any other effect in which one WTG is influencing the production of another WTG.

The state of each WTG at each time is determined through the state transition method, described in Section 2.2.3. A two-state model is used, meaning each WTG is either available or unavailable. If a WTG is available, the output power for the turbine is set as the calculated output value from (2.24) for the current time period. If a WTG is unavailable, the output is naturally set to zero. After determining the state of each WTG, the total power output of the wind farm is calculated with (2.25).

$$P_{wind} = \sum_{j=1}^{\#WTGs} s_j \cdot P(W_s) \quad \text{where} \quad s_j \begin{cases} 1, & \text{if } WTG_i \text{ is available} \\ 0, & \text{if } WTG_i \text{ is unavailable} \end{cases} \tag{2.25}$$

2.3.4 Illustrating Example

As an example, a wind farm consisting of five Vestas V90-2MW turbines is considered. The wind farm is located somewhere where the wind speed characteristics are represented with the Weibull distribution parameters $\alpha = 10$ and $\beta = 2$. The process of computing

the wind farm power output for one hour is described in steps below.

1. A uniformly distributed random number $U = 0.2785$ is generated.

2. The corresponding wind speed is calculated with Equation (2.23), and found to be

$$W_s = 10 \cdot \left(-ln\left(0.2785\right)^{\frac{1}{2}}\right) \text{ m/s} = 11.3064 \text{ m/s}$$

3. Using (2.24), the WTG output at 11.3064 m/s is found to be $P\left(11.3064\right) = 0.8896$ MW.

4. The states of the WTGs are determined by MCS and presented in Table 2.9.

Table 2.9: Availability of WTGs

Unit	s_j
1	1
2	1
3	0
4	0
5	1

5. Equation (2.25) calculates total output power from the wind farm.

$$P_{wind} = (1 + 1 + 0 + 0 + 1) \cdot 0.8896 \text{ MW} = 2.6688 \text{ MW}$$

2.4 Battery Energy Storage System

The intermittent characteristics associated with wind power production highly affect the PSR. Energy storage can retain surplus production and provide reserve energy, thus improving the generation adequacy of a power system with integrated WTG [46]. With the recent advances in battery technology, battery energy storage systems (BESS) have characteristics to be a sustainable solution. The inclusion of BESS introduces intertemporal characteristics into the power system. The main elements in a BESS model are the energy storage balance model and the operation strategy.

2.4.1 Energy Storage Balance Model

The energy storage balance model determines the amount of stored energy and the available charging/discharging energy at all times. The model must include a measurement of current stored energy, PF at each time increment, BESS capacity limits and PF rules [47]. The accuracy of a BESS model can be improved by including considerations of self-discharge, battery degradation and non-linear charge/discharge efficiency [48]. However, the implementation of additional considerations may cause increased model complexity, and large-scale BESS models are often inaccurate in representing the actual operation [49]. Thus, developing a true mathematical BESS model can be complicated.

This thesis applies a simple linear storage model based on [48]. The model neglects self-discharge and battery degradation. The BESS is assumed to be mechanically available at all times, i.e. $FOR_{BESS} = 0$. The BESS is represented with its charging, discharging and capacity values. The charge and discharge limitations are mathematically expressed in (2.26), with the rated charge and discharge capacity $P^{ch,max}$ and $P^{dch,max}$ as the maximum limits, and P_t^{ch} and P_t^{dch} as the charge and discharge rates at time t, respectively.

$$\begin{aligned} 0 \leq P_t^{ch} &\leq P^{ch,max} \\ 0 \leq P_t^{dch} &\leq P^{dch,max} \end{aligned} \tag{2.26}$$

The energy storage limitations of the BESS are expressed in (2.27). E_t denotes the amount of stored energy at time t, expressed in (2.28) with the energy storage balance equation [50].

$$E^{min} \leq E_t \leq E^{max} \tag{2.27}$$

$$E_t = E_{t-1} + \eta^{ch} P_t^{ch} \cdot \Delta t - \frac{P_t^{dch}}{\eta^{dch}} \cdot \Delta t \tag{2.28}$$

In the above equation, Δt is the time increment, e.g. 1 hour or 1 minute, while η^{ch} and η^{dch} represent the charging and discharging efficiencies, respectively. The charge and discharge efficiencies in this thesis is assumed to be ideal, hence $\eta^{ch} = \eta^{dch} = 1$, meaning the above

equation can be rewritten as (2.29).

$$E_t = E_{t-1} + P_t^{ch} \cdot \Delta t - P_t^{dch} \cdot \Delta t \tag{2.29}$$

The storage volume of the BESS is considered to be an integer multiplied with the installed BESS capacity with a charging/discharging period of 6 hours, i.e. a 5 MW battery will have a storage volume of 30 MWh. The available charge and discharge powers at time t are calculated with (2.30) and (2.31).

$$P_t^{ch,ava} = \begin{cases} \frac{E^{max}}{\Delta t} - \frac{E_{t-1}}{\Delta t} & \text{if } 0 \leq \frac{E^{max}}{\Delta t} - \frac{E_{t-1}}{\Delta t} < P^{ch,max} \\ P^{ch,max} & \text{else} \end{cases} \tag{2.30}$$

$$P_t^{dch,ava} = \begin{cases} \frac{E_{t-1}}{\Delta t} - \frac{E^{min}}{\Delta t} & \text{if } 0 \leq \frac{E_{t-1}}{\Delta t} - \frac{E^{min}}{\Delta t} < P^{dch,max} \\ P^{dch,max} & \text{else} \end{cases} \tag{2.31}$$

The model also includes a constraint restricting P_t^{ch} and P_t^{dch} from being nonzero at the same time t, so that the BESS cannot be charged and discharged simultaneously in the model. The constraint is expressed mathematically in (2.32), where P_{sur} is the power surplus from the system, which is dependent on the BESS operation strategy and defined in section 2.4.2.

$$\begin{aligned} P_t^{ch} &= 0 && \text{if } P_{sur,t} < 0 \\ P_t^{dch} &= 0 && \text{if } P_{sur,t} > 0 \\ P_t^{ch}, P_t^{dch} &= 0 && \text{if } P_{sur,t} = 0 \end{aligned} \tag{2.32}$$

2.4.2 Operation Strategies

The operation strategy decides whether the BESS should charge or discharge energy at time t, given energy and storage is available. Thus, the operation strategy is a significant part of the BESS model. This thesis applies four different operation strategies; two strategies aiming to improve system reliability, one with the objective to constrain the RES penetration, and one aiming to smooth the wind power supplied to the system. The four strategies are presented in the following subsections, based on [30].

Strategy 1

In strategy 1, both the power output of the conventional generators and the wind farm can charge the BESS. The surplus from the strategy is calculated with (2.33), where $\sum_{i=1}^{N} P_{i,t}$ is the sum of output power from the N conventional generators at time t.

$$P_{sur,t} = \sum_{i=1}^{N} P_{i,t} + P_{wind,t} - P_{load,t} \tag{2.33}$$

If the total supplied power is larger than the load demand, the surplus energy will be positive and charge the BESS. If the load demand is not satisfied, the system will have negative power surplus and the battery will discharge, given available stored energy.

Strategy 2

Only the wind power can charge the BESS in strategy 2, hence all power produced from the conventional generators can only supply the load. If the wind farm and conventional generators satisfy the load demand, the surplus of wind energy charges the BESS. If load demand is not met by wind and conventional power sources, the battery will discharge to cover the energy deficit. Strategy 2 is expressed in (2.34).

$$\begin{aligned} P_{sur,t} &= P_{wind,t} && \text{if } P_{load,t} \leq \textstyle\sum_{i=1}^{N} P_{i,t} \\ P_{sur,t} &= \textstyle\sum_{i=1}^{N} P_{i,t} + P_{wind,t} - P_{load,t} && \text{else} \end{aligned} \tag{2.34}$$

Strategy 3

To restrict RES penetration level, the sum of power output from the BESS and WTGs at time increment i is not supposed to exceed 15% of the load demand at i. The BESS can only be charged by wind power. If the wind power output is less than 15% of the load, the battery will discharge, given there is available energy. If the wind power surplus is above 15% of the load demand, the wind power surplus will charge the BESS. The surplus of strategy 3 is calculated with (2.35)

$$P_{sur,t} = P_{wind,t} - 0.15 \cdot P_{load,t} \tag{2.35}$$

Strategy 4

Strategy 4 aims to smooth the wind farm output power. The average wind power output $P_{wind,avg}$ over a sample period is calculated. If the wind farm output power is greater than the calculated power average, the BESS is charged by the surplus. If the output power is smaller than the average output power, the BESS discharges to cover the difference. The surplus power of strategy 4 is calculated with (2.36).

$$P_{sur,t} = P_{wind,t} - P_{wind,avg} \tag{2.36}$$

Chapter 3

Methodological Approach

The proposed methodological approaches for obtaining the load model, generation model and ELCC are presented in this chapter.

3.1 Load Model

The load model describes the load variations over a stated period, usually a year. The model accuracy is dependent on the size of the time increments it is divided into. The time increments have equal duration in a model, often either a year, a day or an hour, with varying load levels. The simplest load model is the constant yearly peak load (CYPL) model, with only one time increment and load level over the course of a whole year. This is a pessimistic load model, as the load in reality only is at its peak value a few instances each year. The daily peak load (DPL) model is less pessimistic than the CYPL model, and the hourly peak load (HPL) model even less pessimistic. Thus, finer time resolution gives better load model accuracy [51]. This is illustrated in Figure 3.1.

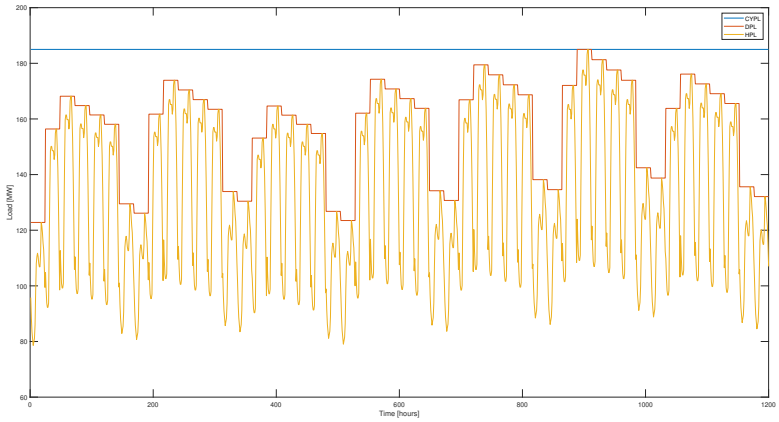

Figure 3.1: Chronological CYPL, DPL and HPL load curve over 50 days.

The load model representation can either be a chronological representation, with the load peak values given at the associated time interval, or as a load duration curve, sorted in descending order from the largest to smallest load [18]. Chronological load representation is required for studies applying sequential simulation techniques. Thus, the load model utilised in this thesis is a chronological HPL model.

3.2 Generation Model Input

To obtain the availability of the conventional generators and the WTGs, the state transition methods need a complete system generation unit list as input. The list must contain the capacity of each generator and the respective failure and repair rates, as illustrated in Table 3.1.

Table 3.1: Generator input for the state transition method.

Generator	**Capacity [MW]**	**Failure rate λ [#/hour]**	**Repair rate μ [#/hour]**
1	$P_{cap,1}$	λ_1	μ_1
2	$P_{cap,2}$	λ_2	μ_1
$\vdots$	$\vdots$	$\vdots$	$\vdots$
n	$P_{cap,n}$	λ_n	μ_1

3.3 Wind Model Input

The model requires the wind data input to be an hourly wind speed series over a whole year in m/s. At time points where no data is registered, the average values of the wind speeds of the previous and following hours are inserted. When deterministic wind data is used, average values for each time increment over several years of wind speed data are calculated to form the input wind speed vector. When Weibull distribution is applied, deterministic data is used to obtain the distribution parameters in order to obtain the cumulative wind speed distribution of the location used in the study, before the input wind speed values are sampled.

3.4 State Transition Method Step-by-Step Guide

The following description of the algorithmic approaches of the state transition MCS method is a recreation of the step-by-step guide created and presented by Øystein Stake Laengen in section 3.2.2.3 *State Transition Method* of his Master's thesis [10], with the exception of points regarding wind power and BESS, which originates from this Master's project. The input data to the script is a list of the n conventional generators of the test systems of the format presented in Table 3.1. The script adds two columns to the list, in order to keep track of the current and next generator states. The n_{WTG} wind turbine generators, with their corresponding MTTF and MTTR, add rows at the bottom of the generator list. A matrix for recording the yearly reliability indices is also created. Note that due to the the short MTTR of the generators, the probability that one or more events happens during one hour is large.

1. Loop through the hours $[1, 8736]$ of simulation year k. The current time increment is denoted i.

   (a) Sample the wind speed of hour i with Weibull distribution based on a generated uniform random number U_{wind} between $[0, 1]$ and input values α and β with (2.23).

   (b) Calculate the power output of each WTG with (2.24) and insert in column 1 of the WTG rows of the generator list.

   (c) A *while* loop runs as long as the next event T_{next} occurs before the next time increment $i + 1$.

      i. Update current state column in generator list with the elements of the next state column.

      ii. Create a transition rate vector based on the information from the current state column elements.

      iii. Calculate the sum of the transition rate vector elements with (2.15).

      iv. Create a probability vector with elements of each possible new generator state with (2.18).

      v. Compute a cumulative probability vector by adding the next state probability to the sum of preceding entries according to Table 2.7.

      vi. Generate a uniformly random number U_1 between $[0, 1]$.

      vii. Decide the next system state by finding the interval in the cumulative probability vector U_1 falls into, as illustrated in Figure 2.7.

      viii. Update the next state column in the generator list with the new system state.

      ix. Generate a uniform random number U_2 between $[0, 1]$.

      x. Calculate the time to next event T_{next} according to (2.20).

      xi. Update the next event time of occurrence to $i + T_{next}$.

   (d) Sum the available generation capacity of conventional generation units at i for all available generators according to the current state column of the n first rows in the generator list.

(e) Sum the available wind generation capacity at i for all available WTGs according to the current state column of the n_{WTG} last rows in the generator list.

(f) Calculate BESS power output based on the power surplus of the system, operation strategy and the equations in Section 2.4.1.

(g) Compare the available generation capacity at i with the load demand at i according to (2.2).

- If the load demand is sufficiently supplied, set the system state to 1 (successful) if the previous system state was 0.
- If the generation capacity is inadequate, count time increment i as a failure. Calculate the energy deficit with (2.3). Set the system state to 0 if the previous system state was 1 and update the frequency counter if so. Calculate and count ΔL with new additional power from BESS according to Figure 2.5.

2. Obtain the LOLE, EENS, LOLF and ELCC indices of year k by using the respective counters.

3. If $i = 8736$, subtract number of hours in a simulation year from the next event time of occurrence $i + T_{next}$.

4. Repeat procedure for the rest of the simulation years.

The PSR indices and CV of the BESS are calculated as the long-term average values of the index counters after processing all the simulation years.

3.5 Illustrative MCS Generation Adequacy Example

To demonstrate the main features of the given algorithmic approach for obtaining the CV of BESS by applying the state transition MCS method, the following illustrative example is presented. In addition, the example demonstrates the difference in calculated CV between $ELCC_{LOLE}$ and $ELCC_{EENS}$. A system consisting of three 100 MW conventional generators, a wind farm with output power capacity of 50 MW and a 30 MW BESS with 60 MWh storage capacity is considered. BESS operation strategy 2 as explained in Section 2.4.2 is applied. The system is evaluated in yearly time increments, with a CYPL demand of 150 MW. The sample size is limited to 10 years since the example is only for illustrative purposes. The yearly power generation, system state, BESS charge and discharge rates, ΔL_{LOLE} and ΔL_{EENS} are presented in Table 3.2. The columns in Table 2.1 provide the following information:

- Column 1 with heading time increment.
- Column 2 is a result of identifying generator states of the system by drawing random numbers.
- Column 3 is the available generation capacity of the conventional generators based on the identified system state.
- Column 4 is the available wind power generation.
- Column 5 is the result of the check if LOL occurs, i.e., LOL occurs if the sum of the values of column 3 and 4 is greater than that of column the constant load demand of 150 MW.
- Column 6 is the energy deficit of the current time increment before the BESS is considered.
- Column 7 is the initial amount of stored energy in the BESS at the beginning of the current simulation year.
- Column 8 is the charging rate of the BESS based on the wind power surplus and amount of stored energy in the BESS.

- Column 9 is the discharging rate of the BESS based on the power surplus of the system and amount of stored energy in the BESS.
- Column 10 is the possible additional load the system can carry with the inclusion of BESS in the generation system if $ELCC_{LOLE}$ is used to assess the CV.
- Column 11 is the possible additional load the system can carry with the inclusion of BESS in the generation system if $ELCC_{EENS}$ is used to assess the CV.

The LOLE and EENS are calculated below with (2.5) and (2.11), respectively.

$$LOLE = \frac{0+1+0+0+0+1+0+0+1+1}{10} = 0.4 \text{ years/year}$$
$$EENS = \frac{0+175200+0+0+0+1138800+0+0+175200+87600}{10}$$
$$= 157680 \text{ MWh/year}$$

The obtained LOLE index of 0.4 years/year means that it is expected that a LOL event is experienced in 2 out of 5 years, while the yielded EENS of 157680 MWh/year gives the expected average annual energy deficit over several years. The $ELCC_{LOLE}$ and $ELCC_{EENS}$ are calculated as the average annual ΔL_{LOLE} and ΔL_{EENS} over the sampling period:

$$ELCC_{LOLE} = \frac{\sum \Delta L_{LOLE}}{\text{\# simulation years}} = \frac{30}{10} \text{ MW} = 3 \text{ MW}$$
$$ELCC_{EENS} = \frac{\sum \Delta L_{LOLE}}{\text{\# simulation years}} = \frac{90}{10} \text{ MW} = 9 \text{ MW}$$

Table 3.2: Illustrative example of applied method in thesis for obtaining CV of BESS.

Year	Generator States	Conventional Generation [MW]	Wind Generation [MW]	LOL	ENS [MWh/year]	Initial E^{BESS} [MWh]	P^{ch} [MW]	P^{dch} [MW]	ΔL_{LOLE} [MW]	ΔL_{EENS} [MW]
1	{1,1,1}	300	50	N	0	0	30	0	0	0
2	{1,0,0}	100	30	Y	175200	30	0	30	10	30
3	{1,0,1}	200	10	N	0	0	10	0	0	0
4	{0,0,1}	100	50	N	0	10	0	0	0	0
5	{0,1,1}	200	0	N	0	10	0	0	0	0
6	{0,0,0}	0	20	Y	1138800	10	0	10	0	10
7	{1,1,1}	300	40	N	0	0	30	0	0	0
8	{1,1,0}	200	20	N	0	30	20	0	0	0
9	{0,1,0}	100	40	Y	175200	40	0	30	20	30
10	{0,1,0}	100	30	Y	87600	20	0	20	0	20

Chapter 4

Case Study

The purpose of the case studies is to assess the CV of BESS in test systems by applying the scripts developed in this thesis. In addition, several sensitivity analyses are conducted to investigate the influence of different system parameters to the BESS CV.

The IEEE Reliability Test System (RTS) and the Roy Billinton Test System (RBTS) are acknowledged test systems in the field of PSR and chosen for this thesis. Both test systems are used for the case studies, while only the RBTS is used for the sensitivity analyses due to time constraints of the project work.

The RBTS is a relatively small composite system developed by the Power Systems Research Group at the University of Saskatchewan in Canada, with aim to be sufficiently small to allow a large number of PSR studies with reasonable solution time while being detailed enough to reflect on the complexity associated with practical reliability studies [52]. It consists of 6 buses, 11 generators with a combined capacity of 240 MW and a peak load of 185 MW. A complete description of the RBTS information required for a generation adequacy assessment using the MCS state transition method can be found in Appendix A.

The RTS is a larger and more complex test system, with objective to [53] "*sufficiently*

broad to provide a basis for reporting on analysis methods for combined generation/transmission (composite) reliability". It was first developed by IEEE in 1979, before it was refined and enlarged in 1986 and 1996 [54]. It consists of 24 buses, 32 generators with a combined capacity of 3405 MW and a peak load of 2850 MW. A complete description of the RTS information required for a generation adequacy assessment using the MCS state transition method can be found in Appendix B.

Both the RBTS and the RTS provide the load data in tables containing weekly, daily and hourly load variations in percent of yearly peak load (YPL) [53]. The supplied load data of the two systems can be found in Appendix C. The HPL of a specific h of day d in week w is calculated by multiplying the weekly, daily and hourly percentage values with the YPL [55], as expressed in (4.1). The chronological HPL curve is obtained with (4.1). The HPL curve will have 8736 load points, as 24 hours/day $\times$ 7 days/week $\times$ 52 weeks/year = 8736 hours.

$$HPL_{h,d,w} = YPL \cdot l_w \cdot l_d \cdot l_h \tag{4.1}$$

where:	$HPL_{h,d,w}$	=	Hourly peak load
	YPL	=	Yearly peak load
	l_w	=	Weekly peak load as a percentage of YPL
	l_d	=	Daily peak load as a percentage of weekly peak load
	l_h	=	Hourly peak load as a percentage of daily peak load

Hourly wind speed data between January 1 2011 to December 31 2016 from Ørland in Norway obtained from the Norwegian Meteorological Institute [56] is used. The corresponding Weibull parameters calculated with the built-in MATLAB function *wblfit* gives $\alpha = 6.0394$ and $\beta = 1.0178$, with associated 95% confidence interval $[5.9883, 6.0909]$ for α and $[1.0101, 1.0254]$ for β.

The capacity of the implemented BESS is the same for both system, in order to investigate the difference of installing the same amount of additional RES power productions in power systems of various sizes.

4.1 RBTS

A wind farm consisting of 30 individual Vestas V90-2MW wind turbines, with a combined power production capacity of 60 MW, is added to the RBTS. The FOR of each individual WTG is assumed to be 0.03, which corresponds to a failure rate of 0.000684932 per hour and a repair rate of 0.022146119 per hour. The installed capacity of the BESS is 20MW and the BESS storage volume is 120 MWh. The charge and discharge capacities are assumed equal. The BESS is assumed to be continuously available. It is assumed that the BESS is completely discharged at the start of each simulation year. The PSR and CV estimates are obtained by simulations of 30,000 years for each strategy, as in [10].

Tables 4.1 and 4.2 show the comparison of RBTS generation adequacy quantification results between the script used in this thesis without wind power contribution and the benchmark results of Billinton and Huang in [51]. The deviation relative to the benchmark values is represented by ϵ, which indicate that the scripts are functioning adequately.

Table 4.1: Obtained LOLE and EENS results of RBTS compared to benchmark values with no wind production.

LOLE [hours/year]			**EENS [MWh/year]**		
Benchmark [51]	Script	ϵ [%]	Benchmark [51]	Script	ϵ [%]
1.0901	1.0858	0.39446	9.9268	9.7316	1.9664

Table 4.2: Obtained LOLF result of RBTS compared to benchmark value with no wind production.

LOLF [occurrences/year]		
Benchmark [51]	Script	ϵ [%]
0.2290	0.2173	5.1092

The system reliability is improved with the integration of the wind farm, with the new LOLE, EENS and LOLF of the system calculated to 0.8015 hours/year, 7.2236 MWh/year and 0.0206 occurrences/year, respectively. In addition, the LOLP has decreased from 0.000124 to 0.000102 with wind power generation integrated.

4.1.1 Strategy 1

The results for $ELCC_{LOLE}$ and $ELCC_{EENS}$ for the RBTS when operation strategy 1 is used is presented in Table 4.3, where σ is the standard deviation of the obtained $ELCC$ values. The CV of the BESS is somewhat higher when calculated based on EENS rather than LOLE. With the LOLE and EENS values of the system being 0.8015 hours/year and 7.2236 MWh/year, it could be expected that the severity of a majority of the LOL events would be within the capacity limits of the BESS. Thus, when a LOL event occurs in the system, the BESS will often contribute with enough power to compensate for the unsatisfied part of the load demand. The $ELCC_{EENS}$ is larger because on the occasions when the BESS cannot prevent the LOL event from occurring, it will most likely reduce the load deficit.

Table 4.3: RBTS results using BESS operation strategy 1.

Method	ELCC [MW]	ELCC [%]	σ [MW]
LOLE	8.548	42.74	30.59
EENS	13.68	68.40	50.12

4.1.2 Strategy 2

Table 4.4 shows the results for $ELCC_{LOLE}$ and $ELCC_{EENS}$ for the RBTS when BESS operation strategy 2 is applied. There is a reduction in the calculated CVs compared to strategy 1, however the reduction is quite small with difference of 4.4% and 4.7% for $ELCC_{LOLE}$ and $ELCC_{EENS}$, respectively. Thus, there is little difference in BESS CV between charging with only wind power versus with all available power when there is a decent amount of wind power penetration in a small and well-designed power system such as the RBTS. As for strategy 1, the estimated $ELCC_{EENS}$ is higher than the $ELCC_{LOLE}$.

Table 4.4: RBTS results using BESS operation strategy 2.

Method	ELCC [MW]	ELCC [%]	σ [MW]
LOLE	8.174	40.87	29.34
EENS	13.04	65.20	47.52

4.1.3 Strategy 3

The estimated $ELCC_{LOLE}$ and $ELCC_{EENS}$ for the RBTS with BESS operation strategy 3 are significantly reduced compared to the results from strategy 1 and strategy 2. The results for operation strategy 3 are shown in Table 4.5. The reduction in CV is most likely due to the RES penetration limitation of covering 15% of the load. The battery capacity seems to be poorly designed for this operation strategy from a PSR point of view, as the BESS is poorly utilised considering prevention of LOL events. Therefore, the BESS capacity should be well-considered when applying an operation strategy where the RES penetration level is constrained if a subobjective is to reduce LOL events in the system. The difference between the obtained $ELCC_{LOLE}$ and $ELCC_{EENS}$ is not as large in strategy 3 as in strategy 1 and strategy 2.

Table 4.5: RBTS results using BESS operation strategy 3.

Method	ELCC [MW]	ELCC [%]	σ [MW]
LOLE	1.219	6.095	6.073
EENS	2.172	10.86	10.64

4.1.4 Strategy 4

The average wind farm output was obtained by simulating 30,000 years and calculated as 9.1707 MW. The results for BESS CV of the RBTS when operating strategy 2 is used are presented in Table 4.6. The results imply that it can be beneficial from a reliability point of view to smooth the wind power output compared to when the aim is to constrain RES penetration level in the system. The $ELCC_{LOLE}$ and $ELCC_{EENS}$ are similar to those of strategy 3, although slightly larger. The CV metrics are significantly lower than for strategies 1 and 2, as expected considering the objective of the different operation

strategies.

Table 4.6: RBTS results using BESS operation strategy 4.

Method	ELCC [MW]	ELCC [%]	sigma [MW]
LOLE	1.844	9.221	8.190
EENS	3.316	16.58	14.80

4.2 RTS

To obtain the same wind power penetration as in the RBTS simulations, in order to be able to cover the load share in operation strategy 3, a wind farm consisting of 425 individual Vestas V90-2MW wind turbines is added to the RTS, with a combined power production capacity of 850 MW. The FOR of each individual WTG is assumed to be 0.03, which corresponds to a failure rate of 0.000684932 per hour and a repair rate of 0.022146119 per hour. The installed capacity of the BESS is 20 MW and the BESS storage volume is 120 MWh. The charge and discharge capacities are assumed equal. The BESS is assumed to be continuously available. It is assumed that the BESS is completely discharged at the start of each simulation year. The PSR and CV estimates are obtained by simulations of 30,000 years for each strategy, as in [10].

Table 4.7 shows the comparison of RTS generation adequacy quantification results between the script used in this thesis without wind power contribution and the benchmark results of Billinton and Huang in [51]. The deviation relative to the benchmark values is represented by ϵ, which indicate that the scripts are functioning adequately.

Table 4.7: Obtained results of RTS compared to benchmark values with no wind production.

LOLE [hours/year]			**EENS [MWh/year]**		
Benchmark [51]	Script	ϵ [%]	Benchmark [51]	Script	ϵ [%]
9.3868	9.4571	0.74892	1192.5072	1181.5559	0.91824

Table 4.8: Obtained LOLF result of RBTS compared to benchmark value with no wind production.

LOLF [occurrences/year]		
Benchmark [51]	Script	ϵ [%]
2.0014	1.9297	3.5825

The system reliability is improved with the integration of the wind farm, with the new LOLE, EENS and LOLF of the system calculated as 6.8995 hours/year, 843.7136 MWh/year and 1.537 occurrences/year. In addition, the LOLP has decreased from 0.001083 to 0.000798 with wind power generation integrated.

4.2.1 Strategy 1

Table 4.9 shows the CV metrics result of the RTS when strategy 1 is used for the BESS operation. The $ELCC_{LOLE}$ is slightly reduced compared to the strategy 1 results for the RBTS. However, the $ELCC_{EENS}$ is severely larger. The main reason for this is the severity of the LOL events, which is indicated with the LOLE and EENS values of 6.8995 hours/year and 843.7136 MWh/year, respectively. The indices imply that the expected energy deficit during a LOL event in the RTS is considerably larger than the installed capacity of the BESS. This can be seen by investigating the maximum amount of energy not served in a year during the simulation, which was 35243 MWh partitioned over 133 LOL events, giving an average LOL severity of 265 MW, considerably larger than the maximum discharge rate of the energy storage. The BESS capacity is therefore not large enough to prevent LOL in a majority of the LOL events, but contributes immensely in reducing the energy deficit of these events.

Table 4.9: RTS results using BESS operation strategy 1.

Method	ELCC [MW]	ELCC [%]	σ [MW]
LOLE	6.930	34.65	14.08
EENS	122.8	614.1	205.6

4.2.2 Strategy 2

The CV results of the BESS in the RTS are presented in Table 4.10. As for the RBTS results, the reduction in the estimated $ELCC_{LOLE}$ and $ELCC_{EENS}$ is small, with difference of 3.7% and 5.2% respectively. The results of the RBTS and RTS imply that the difference between charging with all surplus energy versus only surplus wind energy in a well-designed system with this portion of wind power in the energy mix is little. $ELCC_{EENS}$ is much larger than $ELCC_{LOLE}$, as it was for strategy 1.

Table 4.10: RTS results using BESS operation strategy 2.

Method	ELCC [MW]	ELCC [%]	σ [MW]
LOLE	6.674	33.37	13.67
EENS	116.5	582.4	193.4

4.2.3 Strategy 3

The results for operation strategy 3 are shown in Table 4.11. The CV metrics are significantly reduced compared to strategy 1 and strategy 2, as they were for the RBTS as well. The estimated $ELCC_{LOLE}$ is approximately the same for both test systems, thus the BESS is utilised poorly considering its ability to prevent LOL events in the system. However, it is able to contribute noticeably in reducing the energy deficit relative to the installed BESS capacity, with a $ELCC_{EENS}$ of 21.57 MW.

Table 4.11: RTS results using BESS operation strategy 3.

Method	ELCC [MW]	ELCC [%]	σ [MW]
LOLE	1.136	5.680	4.310
EENS	21.57	107.8	43.39

4.2.4 Strategy 4

The average wind farm output was obtained by simulating 30,000 years and calculated as 9.1707 MW. The CV metrics results of strategy 4 were approximately twice as large as for strategy 3 and can be seen in Table 4.12. The results imply it is better from a PSR point of view when the energy storage is used to smooth the wind power output rather than when the RES penetration level is constrained. As for the results of the RBTS, the $ELCC_{LOLE}$ and $ELCC_{EENS}$ of the RTS with strategy 4 is much lower than for strategy 1 and 2. However, the BESS contributes significantly in reducing the energy deficit in strategy 4 as well.

Table 4.12: RTS results using BESS operation strategy 4.

Method	ELCC [MW]	ELCC [%]	σ [MW]
LOLE	2.084	10.42	6.142
EENS	39.03	195.2	73.47

4.3 Sensitivity Analysis

The sensitivity associated with various system parameters are investigated in this section, in order to understand the applied method and system model to a greater extent. The studies are performed with the RBTS system with BESS operation strategy 2. The input is the same as described in Section 4.1, unless specified otherwise.

4.3.1 BESS Charge and Discharge Capacity

The key issues when planning the integration of a BESS are the storage capacity and limits of the charge and discharge rates. The sensitivities of $P^{ch,max}$ and $P^{dch,max}$ are studied in this subsection, while the storage capacity is considered in the following subsection. The case study results indicate that the implemented BESS is able to cover the energy deficit and prevent possible LOL events. Although a larger discharge capacity instinctively suggests an increased capacity value, as the BESS will be able to cover larger energy deficit, bigger is not necessarily better from a PSR point of view [11]. The change of

$ELCC_{LOLE}$ with the charge and discharge capacity ranging from 1 MW to 40 MW, in steps of 1 MW, is presented in Figure 4.1.

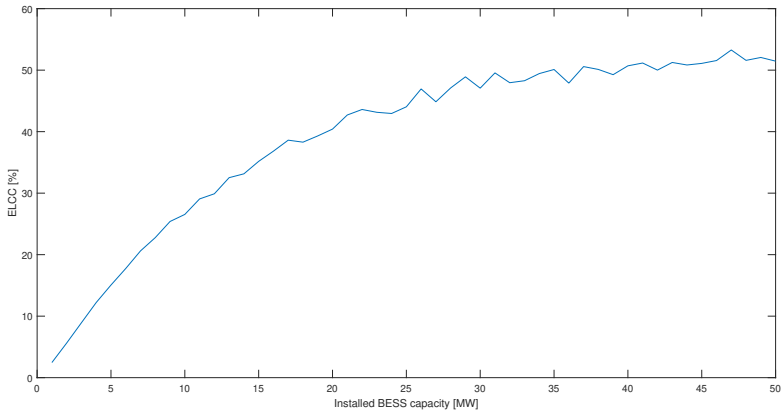

Figure 4.1: The change of $ELCC_{LOLE}$ in percentage of increasingly installed BESS charge/discharge capacity.

The plot demonstrates that the capacity value of BESS increases as the maximum charge and discharge rate limits increase, as the BESS is able to cover greater deficits and prevent more LOL events. As the charge and discharge capacity reaches and exceeds approximately 25 MW, the $ELCC_{LOLE}$ converges towards a value of 50% of the installed charge/discharge cacity. The stabilisation of the relative $ELCC_{LOLE}$, calculated with (2.14), means the specific $ELCC_{LOLE}$ value in MW has a constant increase with the increase of $P^{dch,max}$. The results are in agreement with the findings in [30].

4.3.2 BESS Storage Capacity

As for BESS charge and discharge rate limits, bigger is not necessarily better from a PSR point of view considering storage capacity. The change of $ELCC_{LOLE}$ and $ELCC_{EENS}$ when the storage capacity is increased from $1 \times P^{dch,max}$ to $20 \times P^{dch,max}$, i.e. from a discharge period of 1 hour to 20 hours, is presented in Figure 4.2. The plot suggests no CV dependency of the storage capacity for the RBTS system with the input as described in 4.1. This may be due to the low frequency of LOL events in the system implied by the low LOLE value. Thus, the BESS will in most cases have time to recharge from one LOL

event until the next happens.

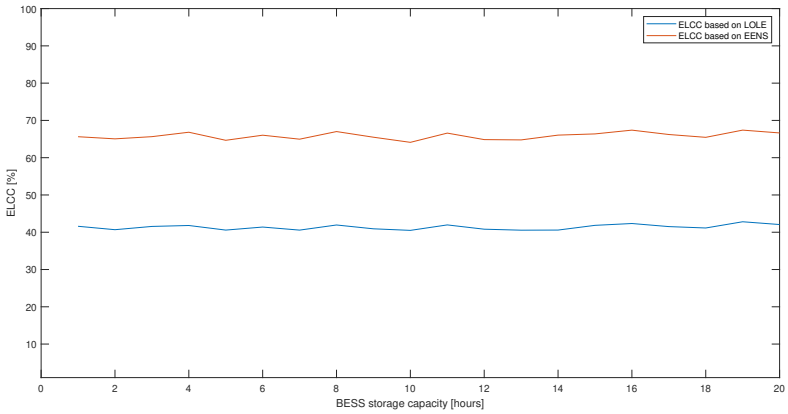

Figure 4.2: The change of $ELCC_{LOLE}$ and $ELCC_{EENS}$ in percentage of installed BESS charge/discharge with increasing BESS storage volume.

To investigate the CV sensitivity to the BESS storage capacity, the RTS is used, as the PSR indices have higher values for it than for the RBTS. The storage capacity is increased from $1 \times P^{dch,max}$ to $10 \times P^{dch,max}$. The resulting plots are presented in Figure 4.3 and Figure 4.4. The plots show that the $ELCC_{LOLE}$ converges before the $ELCC_{EENS}$. Both the $ELCC_{LOLE}$ and the $ELCC_{EENS}$ increase with the growth in BESS storage capacity before converging. The results are in agreement with the findings in [34, 57].

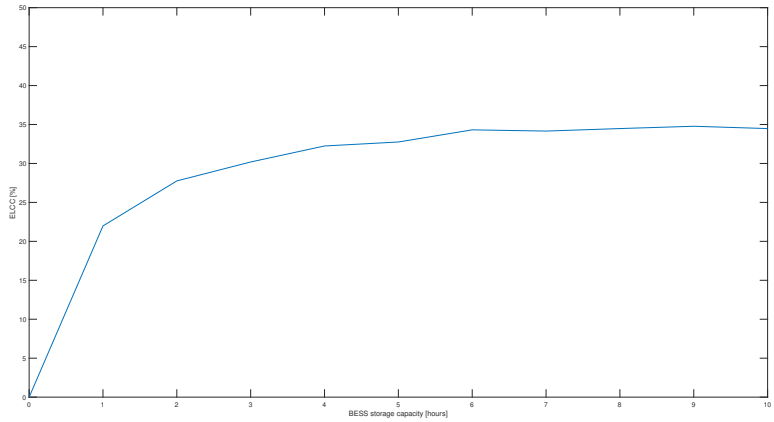

Figure 4.3: The change of $ELCC_{LOLE}$ of the RTS in percentage of installed BESS charge/discharge with increasing BESS storage volume.

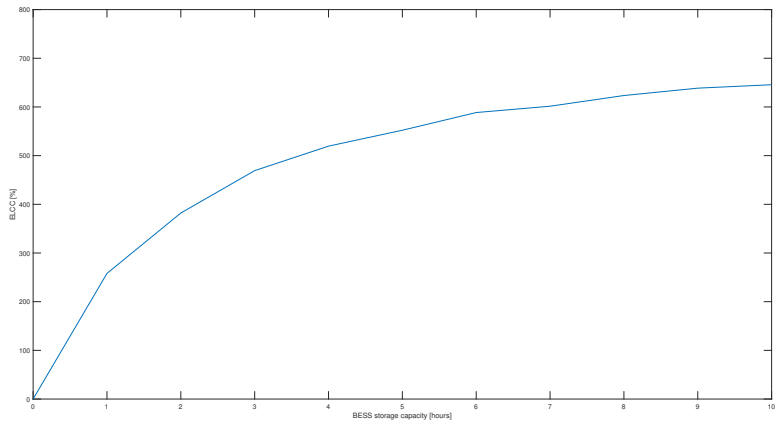

Figure 4.4: The change of $ELCC_{EENS}$ of the RTS in percentage of installed BESS charge/discharge with increasing BESS storage volume.

4.3.3 Size of Wind Farm

The BESS is only charged with power from the wind farm when operation strategy 2 is applied. Intuitively, it can be assumed that the CV of the BESS will decrease if there is a decrease in wind farm power output, as there will be less available energy to charge the battery with. This is examined by increasing the number of wind turbines from 10 to 50,

corresponding to wind farm power capacities of 20 MW and 100 MW in steps of 2 MW. Figure 4.5 shows the change in $ELCC_{LOLE}$ and $ELCC_{EENS}$.

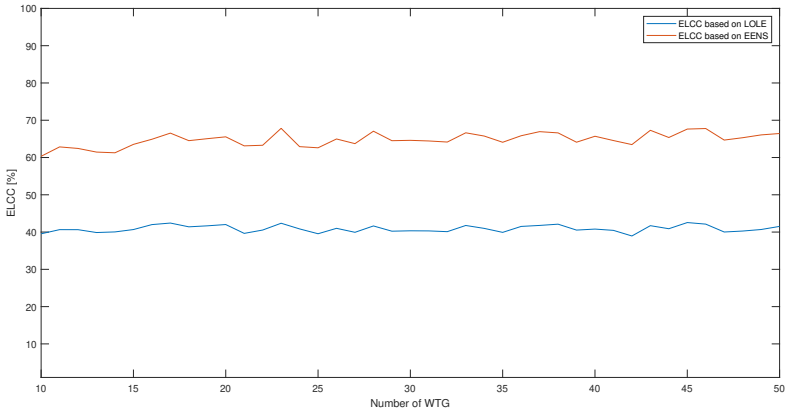

Figure 4.5: The change of $ELCC_{LOLE}$ and $ELCC_{EENS}$ in percentage of installed BESS charge/discharge with number of turbine generators in the wind farm.

The plot presented in Figure 4.5 shows no significant change in CV of the BESS with a change in the number of WTG in the wind farm. The same observations are made by examining the results of increasing the number of turbines from 250 to 600 in the RTS, presented in Figures 4.6 and 4.7. A possible reason is the infrequent occurrence of the LOL events through the year, which indicate that the BESS is able to recharge between the LOL events even when the available charging energy is low. The results are in agreement with the findings in [30].

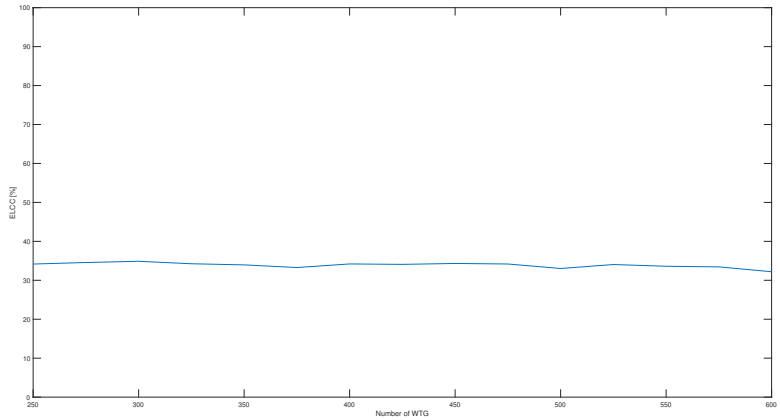

Figure 4.6: The change of $ELCC_{LOLE}$ of the RTS in percentage of installed BESS charge/discharge with number of turbine generators in the wind farm.

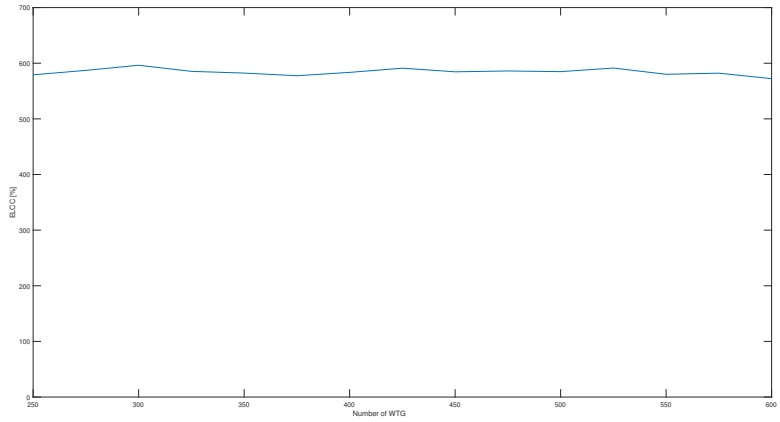

Figure 4.7: The change of $ELCC_{EENS}$ of the RTS in percentage of installed BESS charge/discharge with number of turbine generators in the wind farm.

4.3.4 WTG Availability

Considering the BESS is only charged with power from the wind farm when operation strategy 2 is applied, it can be assumed that the CV of the BESS is sensitive to increasing wind turbine unavailability. This was investigated by calculating the $ELCC_{LOLE}$ relative to the BESS charge and discharge capacity with an increasing wind turbine FOR from

0 to 10%, in steps of 1 %. It was not considered necessary to increase the FOR values beyond 10%, as wind turbines have a high degree of availability [58]. The resulting plot is presented in Figure 4.8. It clearly shows the CV is not influenced by larger FOR values within the studied interval. This can be because of the seldomness of LOL events in the RBTS with additional the 60 MW wind farm implemented, implied by the low LOLE value of 0.8015 hours/year. Thus, the battery will in most cases have time to recharge between the LOL events, even with several WTGs unavailable. Another reason for the approximately unchanged CV may be the relatively high number of wind turbines in the system.

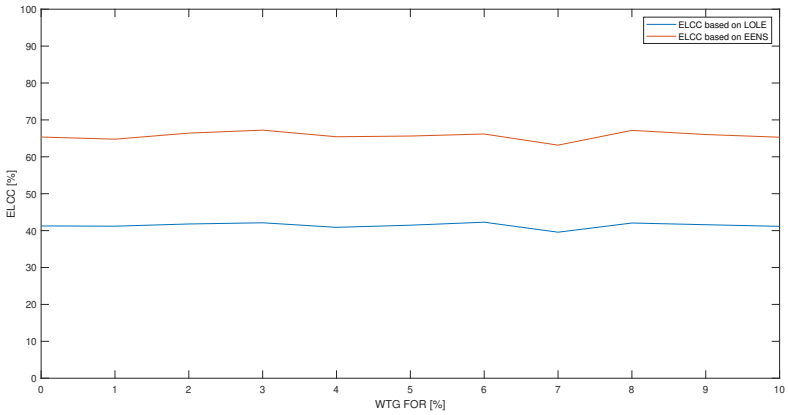

Figure 4.8: The change in $ELCC_{LOLE}$ and $ELCC_{EENS}$ in percentage of installed BESS charge and discharge capacity with increasing WTG FOR.

To investigate sensitivity related to WTG unavailability further, the CV of the BESS in the RTS is calculated with FOR equal to 5% and 10%. The other input values are the same as described in Section 4.2. The resulting $ELCC_{LOLE}$ and $ELCC_{EENS}$ of the different FOR values are compared in Table 4.13. The $ELCC_{LOLE}$ is essentially unchanged, while the $ELCC_{EENS}$ decreases slightly. The results show that the capacity value of BESS is not sensitive to the WTG FOR.

Table 4.13: $ELCC_{LOLE}$ and $ELCC_{EENS}$ of different WTG FOR values.

FOR [%]	3	5	10
$\mathbf{ELCC_{LOLE}}$ **[%]**	33.37	33.12	33.38
$\mathbf{ELCC_{EENS}}$ **[%]**	582.43	579.70	576.21

4.3.5 Peak Load

Obviously, the load demand is significant in a PSR evaluation. The future load demand is uncertain. With a trend of increasing energy consumption in the world, it is interesting to study how well systems manage higher load demand. However, the possibilities concerning distributed and customer-based power production is continuously evolving, which may eventually give a reduction in load demand from a producer and TSO point of view, at least a change in load pattern. Therefore, it can be interesting to investigate how sensitive the CV of the BESS is to a change in load demand. The relative load demand at certain times is presented in Appendix C, with the load level at certain times dependent on the system peak load and calculated with (4.1). Hence, the sensitivity of increasing load is examined by increasing the peak load of the system from 150 MW to 210 MW, with steps of 5 MW. The resulting $ELCC_{LOLE}$ and $ELCC_{EENS}$ are presented in Figure 4.9.

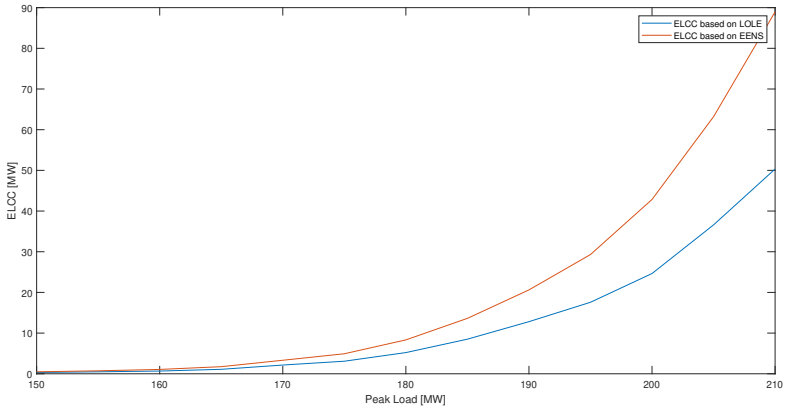

Figure 4.9: The change in $ELCC_{LOLE}$ and $ELCC_{EENS}$ in MW with increasing system peak load.

The CV is close to nought for the lowest load levels, due to a low number of LOL events

in the system per year. Both ELCC values grow increasingly as the system peak load rises, reaching up to $ELCC_{LOLE} = 251.67\%$ and $ELCC_{EENS} = 444.8\%$, or 50.33 MW and 88.96 MW respectively. When the load demand is high, there is an increasing number of LOL events in the system, due to the BESS having several additional opportunities to contribute in satisfying the load demand and is therefore utilised better. To emphasise the potential BESS contribution for the system reliability at higher load levls, the improvement of the LOLE is considered. For the highest load demand, the system LOLE is 5.6769 hours/year. By adding the potential power input from the BESS, with the CV of 50.33 MW, the LOLE is improved to 1.7005. Thus, the BESS can provide substantial contribution in satisfying the load requirement for high load levels for well-designed power systems.

The CV sensitivity to change in the peak load is investigated further by increasing it from 200 MW to 500 MW in steps of 25 MW. During this increase, the reliability level of the system changes from reliable to unreliable, due to the major growth LOL events and energy deficit. The resulting plots are presented in Figure 4.10 and Figure 4.11. Note that the ELCC is given in GW in these figures. Figure 4.10 shows that the $ELCC_{LOLE}$ has a high growth rate up to a peak load of 300 MW. Thus, the BESS is able to contribute in satisfying the load demand and prevent an increasing number of LOL events up to 300 MW. When the peak load surpasses 375 MW, the energy deficit grows too large compared to the BESS capacity and the CV decreases. The change in $ELCC_{EENS}$ in Figure 4.11 shows that the BESS becomes less able to reduce the energy deficit when the peak load grows past 400 MW. This is due to the BESS being discharged an increasingly amount of the time as the peak load increases, as well as having less available energy for charging with all wind farm output power being supplied to the load.

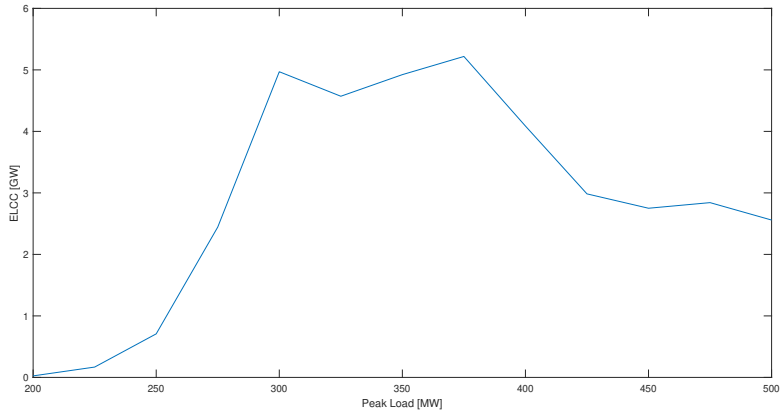

Figure 4.10: The change in $ELCC_{LOLE}$ in GW with increasing system peak load.

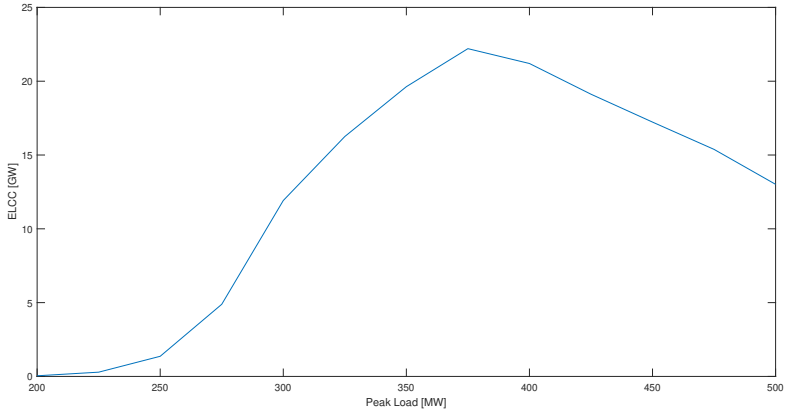

Figure 4.11: The change in $ELCC_{EENS}$ in GW with increasing system peak load.

Chapter 5

Conclusions and Future Work

5.1 Summary of Results

Table 5.1 presents the ELCC results of the different operation strategies for the RBTS and the RTS. It can be observed that the $ELCC_{LOLE}$ values are generally similar in value and size, while the $ELCC_{EENS}$ values from the RTS are approximately ten times larger as for the RBTS results.

Table 5.1: Summary of ELCC results with of different operation strategies for the RBTS and the RTS.

	RBTS		**RTS**	
Operation Strategy	**$\mathbf{ELCC_{LOLE}}$ [MW]**	**$\mathbf{ELCC_{EENS}}$ [MW]**	**$\mathbf{ELCC_{LOLE}}$ [MW]**	**$\mathbf{ELCC_{EENS}}$ [MW]**
1	8.548	13.68	6.930	122.8
2	8.174	13.04	6.674	116.5
3	1.219	2.172	1.136	21.57
4	1.844	3.316	2.084	39.03

5.2 Discussion and Conclusions

This thesis studied and incorporated the algorithmic approaches for CV evaluation of BESS in generation system adequacy assessment through the application of MCS to power systems with wind power integrated. The fundamental theoretical and algorithmic concepts of generation adequacy assessment of power systems with wind power and BESS integrated were examined in the thesis work. The thesis gave a thorough presentation of the applied concepts in order to provide clarity regarding their applications and features. Probabilistic PSR assessment concepts are applied in order to capture the intermittent characteristics of wind power generation, while sequential MCS is a necessity due to the intertemporal features of BESS. The resulting method and MATLAB script applies the traditional probabilistic adequacy indices known as LOLE and EENS to obtain the CV quantification of BESS in form of ELCC metric.

The CV of BESS has been quantified by applying the ELCC metric, which evaluates how much conventional generation capacity the BESS can replace while maintaining the desired reliability level of the system. A significant part of the thesis work was spent on understanding fundamental concepts of CV and the algorithmic aspects of ELCC calculation. The ELCC is obtained by applying the elementary PSR indices LOLE and EENS. The LOLE metric considers expected number of time units in which the system experiences LOL, while the EENS regard the severity of the LOL events. Hence, the ELCC based on EENS gives the CV of the addition generation units ability to reduce the energy deficit, while the ELCC based on LOLE considers only the unit's ability to prevent LOL events. In addition, some time was spent on understanding the methodological approach of sampling wind speed with Weibull distribution. The Weibull probability distribution is often used to characterise wind speed distribution, as it can be modified by the scale and shape parameters to represent many different distributions. The examined concepts and methods were implemented in the existing MATLAB scripts at the Department of Electric Power Engineering for generation adequacy assessment by using MCS.

The resulting MATLAB scripts were applied to calculate the ELCC of the BESS for two

different test systems, the RBTS and the RTS. Four different BESS operation strategies were considered, in which strategies 1 and 2 aim to improve the reliability level, strategy 3 constrains the RES penetration level, and strategy 4 aims to smooth the wind power supplied to the system. It can be observed from Table 5.1 that the ELCC is higher when calculated with EENS than LOLE, due to the EENS metric considering the energy aspect of the LOL events. BESS significantly contributes to overcoming the energy deficit and not necessarily just the reduction of loss of load events, and as such it is imperative that the EENS method be applied for the CV evaluation. Thus, it is preferred to obtain the CV of BESS with methods applying the EENS metric.

The LOLE values of the systems imply that LOL events occur considerably more frequently in the RTS system. However, the calculated $ELCC_{LOLE}$ for the RBTS and RTS have somewhat similar values, with the difference of 6.8-18.92$\%$. This is due to the higher average energy not served per LOL event in the RTS, thus the BESS is not able to cover the entire energy deficit. This is observed by considering the $ELCC_{EENS}$ values for the systems, with the RTS results being approximately 10 times larger than the RBTS results.

The ELCC results of strategies 1 and 2 are considerably better those of strategies 3 and 4, as anticipated. The results demonstrate that the change in the CV of the BESS between operation strategies 1 and 2, hence charging with all available energy versus charging only with surplus wind energy, is small. The differences of the calculated ELCC values are 3.7-4.4$\%$ for $ELCC_{LOLE}$ and 4.7-5.2$\%$ for $ELCC_{EENS}$. The results of strategies 3 and 4 demonstrate that smoothing the wind power supplied to the system with the BESS provide better CV than when the RES penetration level is set to a fixed percentage of the load. However, it should be noted that the ELCC values of strategies 3 and 4 are of the same magnitude.

The results from Section 4.3.1 show that the CV of BESS increase as the maximum charge and discharge capacity increase up to a certain point before converging. Thus, a cheaper BESS with less power capacity can have the same impact on the reliability of the system

as one with larger charge and discharge limits. Similar results can be observed in Section 4.3.2, with the $ELCC_{LOLE}$ and $ELCC_{EENS}$ increasing with the growth in BESS storage capacity before converging in the RTS. However, the results from the RBTS show that the CV of BESS is not sensitive to changes in storage capacity for systems with infrequent occurrence of LOL events.

It can also be observed from the results in Sections 4.3.3 and 4.3.4 that the CV of BESS is neither sensitive to changes in the number of WTGs at the wind farm nor to the availability of the individual WTGs in the RBTS. Thus, the BESS is able to acquire sufficient energy with operation strategy 2 when the amount of available energy from the wind farm is decreased in highly reliable power systems.

Lastly, the peak load sensitivity analysis in Section 4.3.5 shows the effect of increasing load demand on the CV. The ELCC values increase with the peak load while the system is at not highly unreliable. When the peak load increases further and the system becomes unreliable, the energy deficit grows too large and all the power generated by the wind farm is used to cover the load demand, meaning the BESS is not able to charge. Thus, the BESS is able to provide considerable contributions to the system reliability for high load demands, as long as the existing power system has a reasonably good reliability level.

5.3 Future Work

This section presents suggestions of aspects that can form the basis for future research.

5.3.1 Assessment of Composite Systems

This thesis assesses the generation adequacy of power systems. A natural extension of this work would be to use the methodological approach presented for application to composite systems, i.e. HL-II, meaning considerations of load flow, line outages and congestion could be included in the PSR study. Also, there is a possibility to work entirely with analytical methods (say, capacity outage probability tables) instead of using MCS.

5.3.2 State Duration Method

The state transition method is applied in this project. It could be interesting to investigate and compare the performance of other MCS methods. As mentioned, power systems including components with intertemporal characteristics require sequential simulation techniques. Hence, a capacity value study applying the state duration method is a natural continuation of this thesis.

5.3.3 ARMA Wind Speed Sampling

The ARMA time-series model is applied to sample wind speeds in many reliability studies with wind energy resources present. ARMA can be utilised to forecast accurate wind speed data at any particular location. This could give a more robust wind modelling.

5.3.4 Seasonal Wind Variations

The sampling of wind speeds with Weibull distribution in this thesis does not consider the seasonal variations of wind. The wind speed is normally higher in the winter half of the year. By adding seasonal wind variation, the model would be more realistic. It would be interesting to investigate the impact BESS with and without seasonal variations.

If seasonal wind variations were to be included, it could also be interesting to study combinations of different RES. Solar power production could be especially interesting, as wind and solar power are complementary energy sources, with PV solar energy production being higher in the summer half-year. This could allow for higher renewable power penetration. Other intermittent RES can conveniently be implemented in the MATLAB scripts.

5.3.5 Derated Generator States

This thesis uses a two-state model for the conventional generators of the RBTS and the RTS. Generation units can also be available while only allowing a reduced, or derated, value of technical availability. It could be interesting to investigate the effect of including

derated generator states to the capacity value results. This could also give a more realistic and accurate PSR study. The wind farm can be modelled with derated states.

5.3.6 Case Study of Real Power System

This thesis applies the two established PSR test systems, RBTS and RTS, which only are theoretical systems. Conducting a case study of a real power system may allow for further analysis of the methodologies presented in this thesis.

5.3.7 Comprehensive Battery Modelling

The BESS model used in this thesis is a simple linear storage model, where e.g. battery degradation, self-discharge and unavailability are neglected. By adding more considerations, as well as non-linear charge and discharge rates, a more realistic and accurate battery model would be obtained, bearing in mind that too complex energy storage modelling also can lead to inaccuracy.

5.3.8 Different Load Demand Scenarios

The integration of smart components in the power system, as well as the growing opportunities regarding distributed and consumer-based power production, the future load demand pattern and level are uncertain. The RBTS and RTS applies a load demand with a determined sequence, which follows the traditional load patterns. Thus, it would be interesting to study the capacity value of BESS for different load demand scenarios.

5.3.9 Aerodynamic Models for Wind Farms

When wind farms are constructed, the turbines are often clustered together to reduce the costs of installation. This can lead to high wake losses and fatigue loads due to the wake effect in large wind turbine arrays. Optimization of wind farm design and the aerodynamics and aeroelasticity of wind turbines grow more and more important as the installed wind capacity in the world increasing. The wind farm modelling in this thesis does not

take account of the wake effect. By including the wake effect to the wind speed model, a more accurate wind farm power output model could be obtained.

Bibliography

[1] International Renewable Energy Agency - IRENA. *Renewable Capacity Highlights*. https://www.irena.org/-/media/Files/IRENA/Agency/Publication/2019/Mar/RE_capacity_highlights_2019.pdf?la=en&hash=BA9D38354390B001DC0CC9BE03EEE559C280013F, March 2019.

[2] European Environmental Agency. *Renewable energy in Europe - 2018*. https://www.eea.europa.eu/publications/renewable-energy-in-europe-2018, Dec 2018. Accessed: 16.12.2019.

[3] Merriam-Webster. *Intermittent*. https://www.merriam-webster.com/dictionary/intermittent. Accessed: 28.04.2020.

[4] P. D. Lund, J. Lindgren, J. Mikkola, and J. Salpakari. Review of energy system flexibility measures to enable high levels of variable renewable electricity. *Renewable and Sustainable Energy Reviews*, 45:785 – 807, 2015.

[5] R. Irany, A. Kumar, D. Gnoth, and A. Guesmi. *Energy Storage Monitor - Latest trends in energy storage*. Technical report, World Energy Council, Nov 2019.

[6] M. P. Blanco, A. Spisto, N. Hrelja, and G. Fulli. *Generation Adequacy Methologies Review* - eur 27944 en. Technical report, Joint Research Centre Science for Policy Report - European Commission, 2016.

[7] P. Zhang, Ke Meng, and Z.Y. Dong. *Probabilistic vs Deterministic Power System Stability and Reliability Assessment*. Springer-Verlag Berlin Heidelberg, Jan 2010.

[8] R. Billinton and R. N. Allan. *Power-system reliability in perspective*. *Electronics and Power*, 30(3):231–236, March 1984.

[9] M. R. Bhuiyan and R. N. Allan. *Modelling multistate problems in sequential simulation of power system reliability studies*. *IEEE Proceedings - Generation, Transmission and Distribution*, 142(4):343–349, July 1995.

[10] Ø. Stake Laengen. *Application of Monte Carlo Simulation to Power System Adequacy Assessment*. Master's thesis, NTNU, June 2018. Master's thesis.

[11] M. Bjørkeland. *Generation System Adequacy Studies in the Presence of Wind Energy Resources*. Master's thesis, NTNU, Feb 2018. Master's thesis.

[12] International Electrotechnical Commission. *IEV ref 617-01-01*. `http://www.electropedia.org/iev/iev.nsf/display?openform&ievref=617-01-01`, March 2009. Accessed: 19.11.2019.

[13] P. Kundur, J. Paserba, V. Ajjarapu, G. Andersson, A. Bose, C. Canizares, N. Hatziargyriou, D. Hill, A. Stankovic, C. Taylor, T. Van Cutsem, and V. Vittal. *Definition and classification of power system stability IEEE/CIGRE joint task force on stability terms and definitions*. *IEEE Transactions on Power Systems*, 19(3):1387–1401, Aug 2004.

[14] A. Høyland and M. Rausand. *System Reliability Theory : Models and Statistical Methods*. John Wiley & Sons, Incorporated, 1993.

[15] T. Vrana and E. Johansson. *Overview of Analytical Power System Reliability Assessment Techniques*. Technical report, NTNU, May 2011.

[16] A. Solheim. *Incorporating Demand Side Response in Power System Adequacy Studies*. Master's thesis, NTNU, June 2019. Master's thesis.

[17] F. Mohamad, J. Teh, Ching-Ming Lai, and Liang-Rui Chen. *Development of Energy Storage Systems for Power Network Reliability: A Review*. *Energies*, 11:2278, Aug 2018.

[18] R. N. Allan and R. Billinton. *Reliability Evaluation of Power Systems*. Springer Boston, MA, 1996.

[19] D. Elmakias. *New Computational Methods in Power System Reliability*. Springer-Verlag Berlin Heidelberg, 2008.

[20] Wiktionary. *Intertemporal*. `https://en.wiktionary.org/wiki/intertemporal`. Accessed: 16.12.2019.

[21] R. Billinton and W. Li. *Reliability Assessment of Electric Power Systems Using Monte Carlo Methods*. Springer Boston, MA, 1994.

[22] A. Keane, M. Milligan, C. J. Dent, B. Hasche, C. D'Annunzio, K. Dragoon, H. Holttinen, N. Samaan, L. Soder, and M. O'Malley. *Capacity Value of Wind Power*. *IEEE Transactions on Power Systems*, 26(2):564–572, 2011.

[23] R. Sioshansi, S. H. Madaeni, and P. Denholm. *A Dynamic Programming Approach to Estimate the Capacity Value of Energy Storage*. *IEEE Transactions on Power Systems*, 29(1):395–403, 2014.

[24] S. Nolan, M. O'Malley, M. Hummon, S. Kiliccote, and O. Ma. *A methodology for estimating the capacity value of demand response*. In *2014 IEEE PES General Meeting — Conference Exposition*, pages 1–5, 2014.

[25] M. Amelin. *Comparison of Capacity Credit Calculation Methods for Conventional Power Plants and Wind Power*. *IEEE Transactions on Power Systems*, 24(2):685–691, 2009.

[26] L. L. Garver. *Effective Load Carrying Capability of Generating Units*. *IEEE Transactions on Power Apparatus and Systems*, PAS-85(8):910–919, 1966.

[27] Y. Zhou, P. Mancarella, and J. Mutale. *Framework for capacity credit assessment of electrical energy storage and demand response*. *IET Generation, Transmission Distribution*, 10(9):2267–2276, 2016.

[28] R. Billinton, R. Karki, Y. Gao, D. Huang, P. Hu, and W. Wangdee. *Adequacy Assessment Considerations in Wind Integrated Power Systems*. *IEEE Transactions on Power Systems*, 27(4):2297–2305, 2012.

[29] M. Mosadeghy. *Reliability Impacts of Increased Wind Generation in the Australian National Electricity Grid*. Master's thesis, The University of Queensland, 2016. PhD thesis.

[30] N. Shi and Y. Luo. *Capacity value of energy storage considering control strategies*. *PLOS ONE*, 12:e0178466, 05 2017.

[31] C. D'Annunzio. *Generation adequacy assessment of power systems with significant wind generation : a system planning and operations perspective*. Master's thesis, The University of Texas, May 2009. PhD thesis.

[32] R. Billinton and W. Li. *A system state transition sampling method for composite system reliability evaluation*. *IEEE Transactions on Power Systems*, 8(3):761–770, Aug 1993.

[33] S. Shi and K. L. Lo. *Reliability assessment of power system considering the impact of wind energy*. In *2012 47th International Universities Power Engineering Conference (UPEC)*, pages 1–6, 2012.

[34] N. Shi and Y. Luo. *Energy Storage System Sizing Based on a Reliability Assessment of Power Systems Integrated with Wind Power*. *Sustainability*, 9:395, March 2017.

[35] R. Karki, Po Hu, and R. Billinton. *A simplified wind power generation model for reliability evaluation*. *IEEE Transactions on Energy Conversion*, 21(2):533–540, 2006.

[36] A. A. Chowdhury. *Reliability models for large wind farms in generation system*

planning. In *IEEE Power Engineering Society General Meeting, 2005*, pages 1926–1933 Vol. 2, 2005.

[37] R. Billinton and Guang Bai. *Generating capacity adequacy associated with wind energy*. *IEEE Transactions on Energy Conversion*, 19(3):641–646, 2004.

[38] I. Abouzahr and R. Ramakumar. *An approach to assess the performance of utility-interactive wind electric conversion systems*. *IEEE Transactions on Energy Conversion*, 6(4):627–638, 1991.

[39] A. Kadhem, N. I. Abdul Wahab, I. Aris, J. Jasni, and A. Abdalla. *Effect of Wind Energy Unit Availability on Power System Adequacy*. *Indian Journal of Science and Technology*, 9:2–6, July 2016.

[40] M. Tiryakioglu. *On estimating Weibull modulus by moments and maximum likelihood methods*. *Journal of Materials Science*, 43:793–798, Aug 2008.

[41] MathWorks®. *wblfit - Weibull parameter estimates*. `https://se.mathworks.com/help/stats/wblfit.html`. Accessed: 27.04.2020.

[42] A. Sarkar, G. Gugliani, and S. Deep. *Weibull model for wind speed data analysis of different locations in India*. *KSCE Journal of Civil Engineering*, March 2017.

[43] J.V. Seguro and T.W. Lambert. Modern estimation of the parameters of the weibull wind speed distribution for wind energy analysis. *Journal of Wind Engineering and Industrial Aerodynamics*, 85(1):75 – 84, 2000.

[44] Vestas®. *V90-2MW™*. `https://www.vestas.com/en/products/2-mw-platform/v90-2_0_mw#!` Accessed: 27.04.2020.

[45] P. Giorsetto and K. F. Utsurogi. *Development of a New Procedure for Reliability Modeling of Wind Turbine Generators*. *IEEE Transactions on Power Apparatus and Systems*, PAS-102(1):134–143, 1983.

[46] M. Marzband, N. Parhizi, M. Savaghebi, and J. M. Guerrero. *Distributed Smart Decision-Making for a Multimicrogrid System Based on a Hierarchical Interactive Architecture*. *IEEE Transactions on Energy Conversion*, 31(2):637–648, 2016.

[47] K. E. Thorvaldsen. *Energy Storage Modelling*. TET4175 Lecture. Feb 2019, NTNU, Trondheim.

[48] S. Zaferanlouei, M. Korpås, J. Aghaei, H. Farahmand, and N. Hashemipour. *Computational Efficiency Assessment of Multi-Period AC Optimal Power Flow including Energy Storage Systems*. In *2018 International Conference on Smart Energy Systems and Technologies (SEST)*, pages 1–6, Sep 2018.

[49] H. Pandžić and V. Bobanac. *An Accurate Charging Model of Battery Energy Storage*. *IEEE Transactions on Power Systems*, 34(2):1416–1426, March 2019.

[50] L. Nyegaard. *Multi-Period AC Optimal Flow for Distribution Systems with Energy Storage*. Master's thesis, NTNU, June 2019. Master's thesis.

[51] R. Billinton and D. Huang. *Basic Concepts in Generating Capacity Adequacy Evaluation*. In *2006 International Conference on Probabilistic Methods Applied to Power Systems*, pages 1–6, 2006.

[52] R. N. Allan, R. Billinton, I. Sjarief, L. Goel, and K. S. So. *A reliability test system for educational purposes-basic distribution system data and results*. *IEEE Transactions on Power Systems*, 6(2):813–820, 1991.

[53] P. M. Subcommittee. *IEEE Reliability Test System*. *IEEE Transactions on Power Apparatus and Systems*, PAS-98(6):2047–2054, 1979.

[54] C. Grigg, P. Wong, P. Albrecht, R. Allan, M. Bhavaraju, R. Billinton, Q. Chen, C. Fong, S. Haddad, S. Kuruganty, W. Li, R. Mukerji, D. Patton, N. Rau, D. Reppen, A. Schneider, M. Shahidehpour, and C. Singh. *The IEEE Reliability Test System-1996. A report prepared by the Reliability Test System Task Force of the Application of Probability Methods Subcommittee*. *IEEE Transactions on Power Systems*, 14(3):1010–1020, 1999.

[55] K. Koldingsnes. *Reliability-based Derating Approach for Interconnectors*. Master's thesis, NTNU, June 2017. Master's thesis.

[56] Meterologisk Institutt. *Observations - Hourly Data*. http://sharki.oslo.dnmi.no/portal/page?_pageid=73,39035,73_39049&_dad=portal&_schema=PORTAL, 2017.

[57] S. Awara. *On Capacity Value of Energy-Limited Resources in Capacity Markets*. Master's thesis, University of Calgary, April 2019. Master's thesis.

[58] B. Hahn, M. Durstewitz, and K. Rohrig. *Reliability of Wind Turbines*, chapter 8, pages 201–213. Springer-Verlag, Berlin, Heidelberg, 2007. In J. Peinke, P. Schaumann and S. Barth (eds) *Wind Energy*.

[59] R. Billinton, S. Kumar, N. Chowdhury, K. Chu, K. Debnath, L. Goel, E. Khan, P. Kos, G. Nourbakhsh, and J. Oteng-Adjei. *A Reliability Test System for Educational Purposes-Basic Data*. *IEEE Power Engineering Review*, 4(3):1238–1244, Aug 1989.

Appendix A

RBTS

The RBTS is a 6-bus composite system with 9 lines. It was developed for PSR educational purposes at the University of Saskatchewan in Canada with aim to be sufficient small to allow a large number of PSR studies with reasonable solution time whilst being detailed enough to reflect on the complexity associated with practical reliability studies [52]. The generation system consists of 11 generators; 4 thermal generators at bus 1 and 7 hydro generators at bus 2 [59]. The total generation capacity of the system is 240 MW, with the individual generator capacity ranging from 5 MW to 40 MW. The capacity, FOR and failure/repair rate of each generator is shown in Table A.1. The system load is partitioned in buses 2-6, with a total system peak load of 185 MW. The RBTS connections and the peak load of the different buses are shown in Figure A.1.

Table A.1: RBTS generator data [59].

Capacity [MW]	Bus [#]	FOR	#fail/hour [1/hour]	#rep/hour [1/hour]
10	1	0.020	0.000456621	0.022374429
20	1	0.025	0.000570776	0.022260274
40	1	0.030	0.000684932	0.022146119
40	1	0.030	0.000684932	0.022146119
5	2	0.010	0.000228311	0.02260274
5	2	0.010	0.000228311	0.02260274
20	2	0.015	0.000273973	0.017990868
20	2	0.015	0.000273973	0.017990868
20	2	0.015	0.000273973	0.017990868
20	2	0.015	0.000273973	0.017990868
40	2	0.020	0.000342466	0.016780822

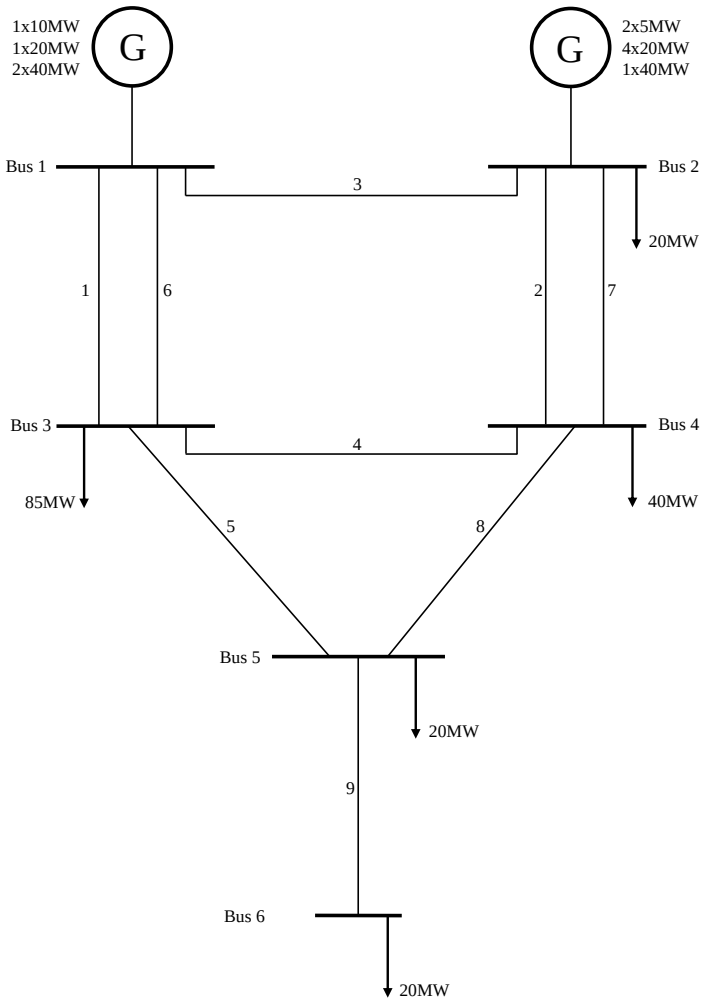

Figure A.1: RBTS single line diagram [59].

Appendix B

RTS

The RTS is a 24-bus PSR test system with 38 lines. It was originally developed in 1979 with objective to [53] "*sufficiently broad to provide a basis for reporting on analysis methods for combined generation/transmission (composite) reliability*", and later refined and expanded in 1986 and 1996 [54]. The generation system consists of 32 generators based on hydro, coal, oil and nuclear energy, with a production capacity ranging from 12 MW to 400 MW. The total system generation capacity is 3405 MW. The RTS generator data is presented in Table B.1. The system load is divided between 16 buses with a total peak value of 2850 MW. The RTS single line diagram is illustrated in Figure B.1.

Table B.1: RTS generator data [54].

Capacity [MW]	Bus [#]	FOR	#fail/hour [1/hour]	#rep/hour [1/hour]
12	15	0.02	0.00034014	0.01666667
12	15	0.02	0.00034014	0.01666667
12	15	0.02	0.00034014	0.01666667
12	15	0.02	0.00034014	0.01666667
12	15	0.02	0.00034014	0.01666667
20	1	0.1	0.00222222	0.02
20	1	0.1	0.00222222	0.02
20	2	0.1	0.00222222	0.02
20	2	0.1	0.00222222	0.02
50	22	0.01	0.00050505	0.05
50	22	0.01	0.00050505	0.05
50	22	0.01	0.00050505	0.05
50	22	0.01	0.00050505	0.05
50	22	0.01	0.00050505	0.05
50	22	0.01	0.00050505	0.05
76	1	0.02	0.0005102	0.025
76	1	0.02	0.0005102	0.025
76	2	0.02	0.0005102	0.025
76	2	0.02	0.0005102	0.025
100	7	0.04	0.00083333	0.02
100	7	0.04	0.00083333	0.02
100	7	0.04	0.00083333	0.02
155	15	0.04	0.00104167	0.025
155	16	0.04	0.00104167	0.025
155	23	0.04	0.00104167	0.025
155	23	0.04	0.00104167	0.025
197	13	0.05	0.00105263	0.02
197	13	0.05	0.00105263	0.02
197	13	0.05	0.00105263	0.02
350	23	0.08	0.00086957	0.01
400	18	0.12	0.00090909	0.00666667
400	21	0.12	0.00090909	0.00666667

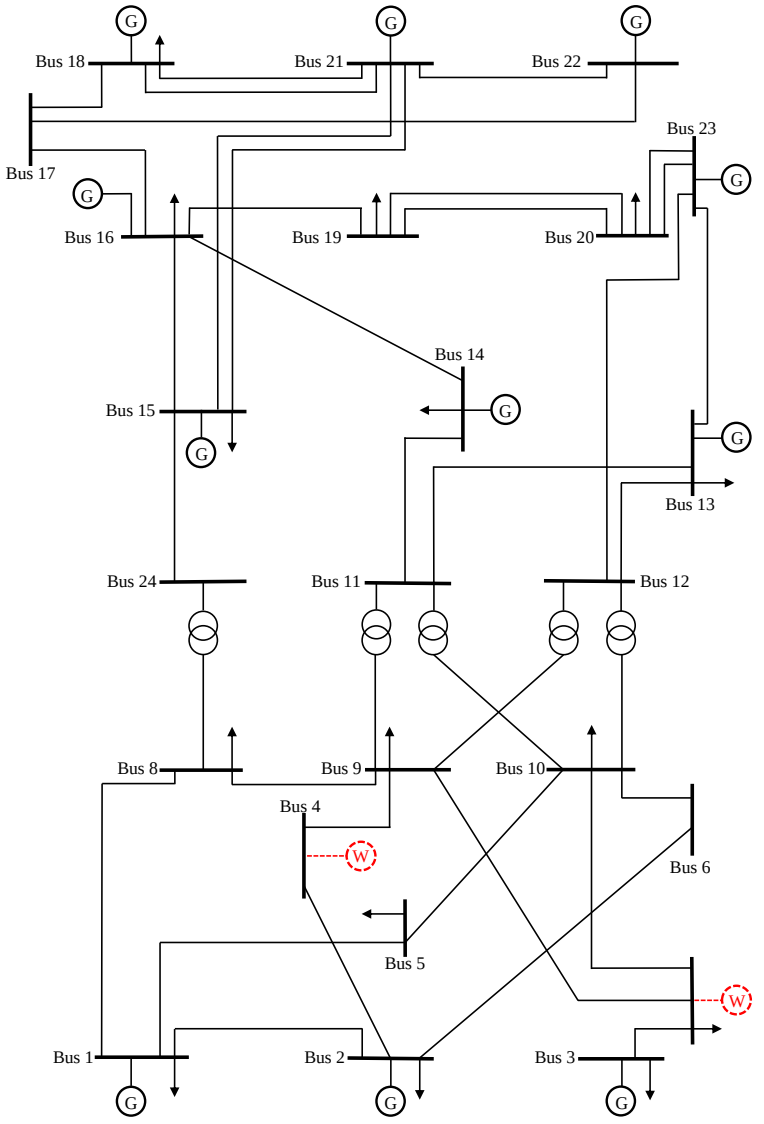

Figure B.1: RTS single line diagram [54].

Appendix C

Load Data

The load data input of the RBTS and the RTS from [54] is presented in Table C.1, C.2 and C.3.

Table C.1: DPL data.

Day	DPL [% of WPL]
Monday	93
Tuesday	100
Wednesday	98
Thursday	96
Friday	94
Saturday	77
Sunday	75

Table C.2: WPL data.

Week	WPL [% of YPL]	Week	WPL [% of YPL]	Week	WPL [% of YPL]	Week	WPL [% of YPL]
1	86.2	14	75	27	75.5	40	72.4
2	90	15	72.1	28	81.6	41	74.3
3	87.8	16	80	29	80.1	42	74.4
4	83.4	17	75.4	30	88	43	80
5	88	18	83.7	31	72.2	44	88.1
6	84.1	19	87	32	77.6	45	88.5
7	83.2	20	88	33	80	46	90.9
8	80.6	21	85.6	34	72.9	47	94
9	74	22	81.1	35	72.6	48	89
10	73.7	23	90	36	70.5	49	94.2
11	71.5	24	88.7	37	78	50	97
12	72.7	25	89.6	38	69.5	51	100
13	70.4	26	86.1	39	72.4	52	95.2

Table C.3: HPL data.

Hour	Winter weeks 1-8 & 44-52		Summer weeks 18-30		Spring/Fall weeks 9-17 & 31-43	
	Weekday [% of DPL]	Weekend [% of DPL]	Weekday [% of DPL]	Weekend [% of DPL]	Weekday [% of DPL]	Weekend [% of DPL]
1	67	78	64	74	63	75
2	63	72	60	70	62	73
3	60	68	58	66	60	69
4	59	66	56	65	58	66
5	59	64	56	64	59	65
6	60	65	58	62	65	65
7	74	66	64	62	72	68
8	86	70	76	66	85	74
9	95	80	87	81	95	83
10	96	88	95	86	99	89
11	96	90	99	91	100	92
12	95	91	100	93	99	94
13	95	90	99	93	93	91
14	95	88	100	92	92	90
15	93	87	100	91	90	90
16	94	87	97	91	88	86
17	99	91	96	92	90	85
18	100	100	96	94	92	88
19	100	99	93	95	96	92
20	96	97	92	95	98	100
21	91	94	92	100	96	97
22	83	92	93	93	90	95
23	73	87	87	88	80	90
24	63	81	72	80	70	85

Appendix D

MATLAB Script

(Restricted Public Access)

Håvard Dahl Mediaas

Contribution of Energy Storage to Generation Adequacy

NTNU
Norwegian University of
Science and Technology